

The interactions of instabilities during miscible CO₂ enhanced oil recovery: A numerical simulation study

P. Ogbeiwi^{1,*}. K. D. Stephen¹

¹ Institute of Geoenergy Engineering, Heriot-Watt University, Edinburgh EH14 4AS, UK

prejohn73@gmail.com, <https://orcid.org/0009-0009-4383-5685>

This manuscript has been prepared for publication in **Fuel**. Please note that the manuscript will undergo peer review and is yet to be formally accepted for publication. Subsequent versions of this manuscript may have slightly different content. Please feel free to contact the corresponding author; we welcome feedback

Abstract

During field-scale simulations of miscible displacements, the effect of heterogeneity-induced channelling is always accounted for, while micro-scale physical instabilities like viscous fingering and molecular diffusion are ignored due to the computational costs of the required fine-grid simulations. Thus, the interplay between small- and macro-scale physical instabilities is not properly understood. In this study, we examined the interactions of the small- and macro-scale effects during miscible CO₂ displacements using two-dimensional, inter-well scale, fine-grid models. Using the linear stability theory, we described the fingering behaviours of a set of homogeneous models which were perturbed initially to artificially seed different forms of fingers. We also attempted to identify the range of permeability variation in a set of heterogeneous models at which the effect of viscous fingering or physical diffusion diminishes, and the permeability heterogeneity dominates the process. Our results showed that in models with little or no heterogeneity, viscosity fingering, and physical diffusion exerted control on the dynamics of the flooding process. However, as the degree of heterogeneity increased, the influence of viscous fingering and diffusion diminished, with a corresponding increase in the influence of permeability heterogeneity/variation. Overall, during miscible displacements, oil recovery and CO₂ storage were improved because of the interactions of diffusive forces, viscous fingering and/or reservoir heterogeneity.

Keywords Viscous fingering · Miscible displacements · Heterogeneity · CO₂ enhanced oil recovery · Diffusion

1 Introduction

Petroleum reservoirs are considered suitable for CO₂ storage and enhanced oil recovery because that they have a geologic seal which has trapped hydrocarbons for a long period of time. The geological properties of the reservoirs are fairly known, and this reduces the amount of associated uncertainties and risks when compared to other forms of CO₂ storages (Stewart et al., 2018a). Also, CO₂ injection leads to incremental oil production which provides economic benefits to offset the costs associated with carbon capture and storage.

CO₂ injection can be classed as miscible, near-miscible, or immiscible flooding depending on the pressure of displacement, temperature, and the characteristics of the in-situ fluid. The efficiency of miscible CO₂ enhanced oil recovery (EOR) during miscible and immiscible displacement depends on the microscopic (local) as well as macroscopic (areal and vertical) sweep performance. The microscopic efficiency is a function of molecular diffusion and dispersion of the injection gas which affects the degree of mixing between the injected and in-situ fluid. This efficiency is typically high because of the low interfacial tension (IFT) between the fluids as well as density and viscosity reduction. On the macroscopic scale, numerous physical factors affect the displacement efficiency and ultimate oil recovery from a CO₂ injection process (Blunt et al., 1993; Orr, 2004). They include permeability heterogeneities in the formation rock, segregation of injected fluids due to gravity, gas channelling and fingering leading to the instability of the displacement front. These large-scale factors affect the displacement efficiency and ultimate oil recovery from a CO₂ injection process.

For CO₂ injection to be efficient in terms of both microscopic and macroscopic displacement, it is essential to maintain a low mobility ratio value. Generally, the mobility ratio of a typical CO₂ gas flood varies from 20 to 100% due to the low viscosity of CO₂ (Jaber & Awang, 2017; Moghadasi et al., 2018). These unfavourable mobility ratio values cause higher instabilities of the displacement front, unstable pressure distribution and a greater tendency for the occurrence of viscous fingering where CO₂ fingers through the reservoir bypassing oil in the process (Blunt et al., 1993; Jaber & Awang, 2017). Consequently, this leads to an early injected gas breakthrough and low incremental oil recoveries (Aghdam et al., 2013; Moghadasi et al., 2018).

Macroscopically, reservoir rocks (sedimentary rocks) may occur in layers with uncorrelated flow characteristics due to the variation in the depositional environments. This gives rise to the phenomenon of reservoir permeability heterogeneity which can be present in different layers or strata of the formation, resulting in different homogenous layers or zones within the oil pay which have individual permeability. The impacts of stratification and permeability heterogeneity vary for different reservoirs, but they clearly affect important reservoir parameters such as capillary pressure, phase saturations, mobility ratios and relative permeabilities (Zahoor et al., 2011). Also, reservoir heterogeneity can cause significant variations in the reservoir's vertical and horizontal permeability making the reservoir fluid flow behaviour disordered and complex to model.

In CO₂ EOR, the presence of reservoir heterogeneity adversely affects the performance of the process in two ways. Firstly, there is the presence of thief zones or highly permeable channels which leads to problems of large volume of injected fluids being recovered with correspondingly low oil recoveries. This is because the injected fluid preferentially travels through the high permeability channels bypassing oil in the process and resulting in a relatively early breakthrough of the injected gas (Stewart et al., 2018b). Secondly, in the presence of low vertical-to-horizontal permeability ratio, the low permeability channels remain unswept which may further reduce the oil recovery efficiency and increase gas production. This significantly decreases the storage capacity and the displacement efficiency of the injected fluid (Ghaderi et al., 2013).

In general, the bypassing of the reservoir oil by the injected gas in CO₂ EOR can be classified into viscous fingering and channelling of the injected gas. The former occurs as a result of viscosity – driven instability arising from the unfavourable viscosity ratio of the injected and in-situ fluids while the latter is caused by the heterogeneity of porous media. The effect of channelling is more noticeable in the presence of viscous fingering due to the adverse mobility ratio between the injected gas and oil. Also, the presence of heterogeneity can trigger fingers and advance their subsequent growth. Hence to adequately model the dynamics of the miscible displacement process, it is necessary to quantify the interplay between physical instabilities such as viscous and gravitational fingering, and inherent reservoir heterogeneity, and how these phenomena affect the performance of the flood.

Some studies have been carried out to assess the effects of fingering and heterogeneity on secondary and enhanced oil recovery processes. A study by (Brock & Orr Jr., 1991) carried out flow experiments and numerical simulations to examine the combined effects of viscous fingering and permeability heterogeneity in various 2D glass bead packs. Their results showed that the degree of connectivity of the varying permeability zones e.g., the structure of the layers or thief zones has a significant effect on the unstable flow process, while the presence of heterogeneities in some scenarios affect the location and paths of the fingers. However, they indicated that the flow patterns were also affected by viscous fingering. However, this effect was not assessed in detail. In their study, (Tchelepi & Orr, 1994) applied numerical simulation to investigate the interplay of viscous fingering, heterogeneity of permeability and gravity override in miscible-gas-injection processes in three-dimensional reservoir models. Their results indicated the significance of the effects of permeability heterogeneity on the propagation of the miscible gas. A study by (Luo et al., 2017) examined the interactions of fingering and channelling in the upscaling of polymer EOR in oil reservoirs with high oil viscosities. In their study, (Chang et al., 1994) carried out reservoir simulations with unstable flow which took the effects of different heterogeneities at the field scale into account. Their results showed that together with the effects of the mobility ratio, the flow was dominated by channelling at the field scale and by viscous fingering at the microscale.

In some of these studies, the effects of small-scale physical instabilities such as viscous fingering are ignored because of the large computational requirements of high resolution fine gridded simulations and the complexities

associated with the fine-scale structure of the gas fingers and the miscible front (Luo et al., 2017). As a result, the effects of channelling due to permeability-induced heterogeneity was said to dominate in unstable fluid displacement process. This leads to inherent errors in large scale simulations as well as an incomplete understanding of the processes of fluid flow and oil recovery. Viscous fingering is a microscopic effect which affects the displacement efficiency of the unstable flow process at the pore scale. Therefore, the effects of the interactions between viscous fingering and heterogeneity on miscible displacements have not been fully understood. During miscible CO₂ flooding, viscous fingering and permeability heterogeneity interact to determine the sweep efficiency of the flood. Also, since real reservoirs contains permeability heterogeneities at many scales, it is necessary to understand the interactions of viscous fingering and heterogeneity and determine the effect of each factor on the overall performance of the displacement process.

In this study, we quantified the interactions of the effects of viscous fingering and permeability heterogeneity during miscible CO₂ enhanced oil recovery. We do so by attempting to identify if a range of permeability heterogeneity of a reservoir model exists at which viscosity-induced instabilities has an insignificant effect on the flow displacement process and the overall performance of the flood, and at which the miscible displacement process is entirely dominated by the permeability heterogeneity within the reservoir rock. We ask the question: How does the interplay between fingering as a result of viscosity contrast and channelling due to permeability heterogeneity describe the spatial migration of the injected gas, the storage of CO₂ and the recovery of oil in a CO₂ EOR process? The porous media considered consists of two sets of two-dimensional x - z inter-well reservoir scale models which include a homogeneous reservoir model, and a stratified model with low vertical communication described by a low vertical-to-horizontal permeability ratio (k_v/k_h). The effects of gravity segregation are not considered in this study because of the low k_v/k_h ratio of the porous media employed. According to (Zahoor et al., 2011), gravity segregation does not dominate the fluid flow behaviour in reservoirs with low k_v/k_h ratio.

2 Modelling the interactions of viscous fingering and permeability heterogeneity in miscible CO₂ enhanced oil recovery: The methodology.

2.1 Flow Equations

Compositional fluid models capture and model the complicated interactions between fluid flow and phase behaviours (Moortgat et al., 2012). In compositional models, the real compositions of oil and gas phases due to their complex fluid behaviour is explicitly acknowledged. Therefore, equations of state computations and interactions between the components must be adequately represented. A finite number of components, N_c , must be utilised to denote the reservoir fluid composition (Chen et al., 2006). Given that ξ_{io} and ξ_{ig} represent the molar densities of component i in the liquid and gas phases, and M_i connotes the molecular weight of the component i , then:

$$\xi_{i\alpha} = \frac{\rho_{i\alpha}}{M_i}, \quad i = 1, 2, 3, \dots, N_c \text{ and } \alpha = o, g \quad (1)$$

where $\rho_{i\alpha}$ represents the mass density the phase α . Therefore, the molar density of the phase α is given as:

$$\xi_{\alpha} = \sum_{i=1}^{N_c} \xi_{i\alpha}, \quad \alpha = o, g \quad (2)$$

The mole fraction of component i in phase α is given as:

$$x_{i\alpha} = \frac{\xi_{i\alpha}}{\xi_{\alpha}}, \quad i = 1, 2, 3, \dots, N_c \text{ and } \alpha = o, g \quad (3)$$

In compositional simulations, mass exchange occurs between phases, and therefore the mass within each phase is not conserved like is done in black-oil models. The total mass conversation occurs instead for each component and is given as (Chen et al., 2006):

$$\frac{\partial(\phi\xi_w S_w)}{\partial t} = -\nabla \cdot (\xi_w v_w) + q_w \quad (4)$$

$$\frac{\partial(\phi[x_{io}\xi_o S_o + x_{ig}\xi_g S_g])}{\partial t} = -\nabla \cdot (x_{io}\xi_o v_o + x_{ig}\xi_g v_g) - \nabla \cdot (d_{io} + d_{ig}) + q_i \quad (5)$$

where q_w and q_i are the respective molar flowrates for water and the i^{th} component, $d_{i\alpha}$ represents the diffusive flow of the i^{th} component in the α -phase. Darcy's law for the respective phases can be written as:

$$v_\alpha = \frac{k_{r\alpha}}{\mu_\alpha} K (\nabla P_\alpha - \rho_\alpha \gamma \nabla z) \quad \alpha = w, o, g \quad (6)$$

where k_r , μ and ∇P represents the relative permeability, viscosity and pressure gradient of the respective phases. Also, K , γ and ∇z represent the permeability, gravity term, and change in vertical distance, respectively.

Equations 7, 8 and 9 below are the mathematical constraints which must be observed for the saturations, phase pressures balance, and mole fractions, respectively (Chen et al., 2006).

The saturations of each phase are such that:

$$S_o + S_w + S_g = 1 \quad (7)$$

Capillary pressure, P_c is used to relate the phase pressures, such that:

$$P_{cow} = P_o - P_w, \text{ and } P_{cgo} = P_g - P_o \quad (8)$$

$$\sum_{i=1}^{N_c} x_{i\alpha} = 1 \quad (9)$$

In this study a compositional simulation was used to model the multi-contact miscible displacement process (Al-Mudhafar et al., 2018; Esmail et al., 2007; Naderi & Simjoo, 2019; Vahidi et al., 2014). This is because they can predict the phase behaviour as well as the displacement behaviour in the reservoir.

2.2 Two-Dimensional Inter-well Reservoir Models

We built two-dimensional (2D) cross-sectional models which represent an inter-well scale of the reservoir models. Very small perturbations were applied to permeability in the column of cell at the injection well to seed viscous fingering and create different realisations. A schematic of the 2D reservoir model is shown in Figure 1.

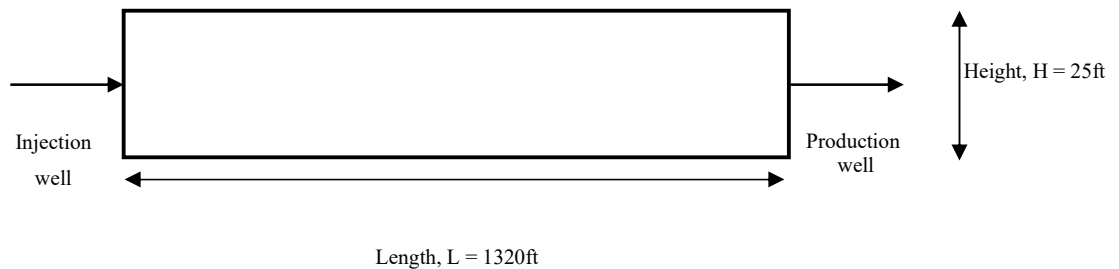


Figure 1: The 2D model used throughout the study. The injection and production wells are located on the left- and the right-hand side of the reservoir, respectively. Also, no flow boundaries are imposed at the top and bottom of the model, and the mean flow is in the x-direction.

The reservoir simulation model was a 2D cross-sectional model which represented a volume of the reservoir between a gas injector and a production well. The injector and producer were set at opposite ends of the model and completed along the length of the model. The average porosity was 34.4%, the average horizontal permeability was set at 721mD, and the average vertical permeability was 2.524mD. Due to the low vertical to horizontal permeability ratio, the model was highly stratified, and the effects of gravity crossflow were minimal.

The cells of the model had sizes of 5 x 70 x 1ft and the model consisted of 264 x 1 x 25 grid blocks, making 6600 grid blocks in total. The water, gas, and oil viscosities were 0.613, 0.175, and 1.33 centipoise respectively, resulting in a relatively favourable mobility ratio between oil and water during water injection and a relatively unfavourable mobility ratio between the oil and CO₂ during CO₂ injection. A summary of rock and fluid properties of the model are provided in Table 1.

Table 1: Rock and fluid properties applied in the numerical simulation.

<i>Property</i>	<i>Value</i>
Number of cells	264 x 1 x 25
Grid block size, ft.	5 x 70 x 0.48
Average porosity, ϕ (%)	34.4
Initial water saturation, S_w (%)	20
Average horizontal permeability, k (mD)	721
Average vertical permeability, k (mD)	2.524
Initial reservoir pressure, P_R (psia)	1950
Initial reservoir temperature, °F	110
Oil viscosity, μ_o (cP)	1.33
Water viscosity, μ_w (cP)	0.613
CO ₂ viscosity, μ_g (cP)	0.175

The water-oil and gas-oil relative curves are shown in Figure 2. No flow boundaries were imposed at the top and bottom of the model and the reservoir was initially saturated with the seven-component oil and connate water. Waterflooding was first performed for 720 days to bring oil saturation to a residual value. The injection of pure CO₂ was then carried out for 600 days in a tertiary flood. The injector well was operated at a fixed BHP of 3000 psi and a target injection rate of 100stb/day and 580Mscf/day during the water and gas injection phases, respectively, representing a reservoir injection rate of 1.97 PV/year, while the producer was operated at a constant flow rate of 100 stb/day. The typical run-time of the two-dimensional model is 0.5 hours of CPU time.

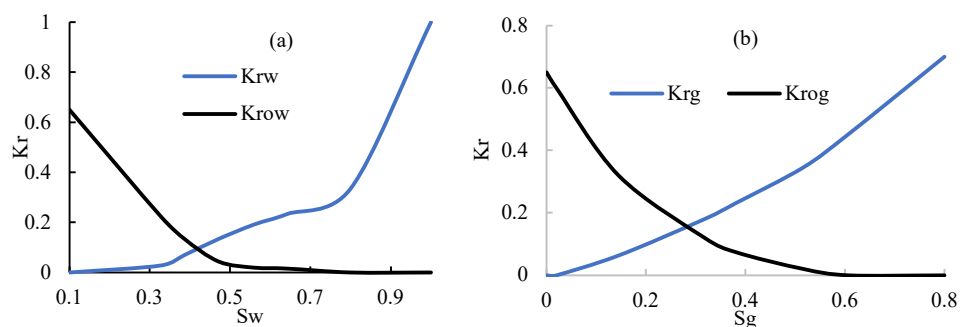


Figure 2: Relative permeability curves for the (a) oil-water, and (b) gas-oil system

2.2.1 Compositional Fluid Model

In this study, compositional fluid model was applied to characterise the phase behaviour and fluid properties of the system. The compositional model was generated using the Schlumberger ECLIPSE reservoir simulation software which was applied to simulate reservoir fluid flow and phase behaviour during CO₂ enhanced oil recovery.

The compositional model was lumped into seven components and a modified Peng-Robinson Equation of State (EOS) is applied to the study. The composition of the initial oil is given in Table 2. Table 3 presents the PVT parameters used in this study. The minimum miscibility pressure (MMP) of the reservoir oil with CO₂ was calculated using the Glasø correlation (Glasø, 1985) of the Schlumberger PVTi software (2019) as 80.7 bars (approximately 1170.46 psia).

Table 2: Composition of the initial oil

Component	CO ₂	C ₁	C ₂ –nC ₄	iC ₅ –C ₆	HYP1	HYP2	HYP3
Initial oil (%)	1.18	11.7	19.5	22	28.2	9.4	8.1

Table 3: EOS parameters for the different components of the fluid model

Component Names	CO ₂	C ₁	C ₂ -nC ₄	iC ₅ -C ₆	HYP01	HYP02	HYP03
Molecular Weights (g/mol)	44.01	16.04	38.4	72.82	135.82	257.75	330.998
Omega A	0.457	0.457	0.457	0.457	0.457	0.457	0.457
Omega B	0.078	0.078	0.078	0.078	0.078	0.078	0.078
Critical T (K)	376.244	215.626	353.668	469.3	621.341	779.695	847.748
Critical P (bar)	47.73	81.303	51.576	35.747	25.142	13.861	10.318
Acentric Factors	0.142	0.47	0.136	0.224	0.438	0.837	1.056
Volume Shift	-0.083	0.074	-0.086	-0.043	0.022	0.226	0.334
Component Parachors	153.228	74.912	137.52	233.896	393.596	662.45	843.128
Mol Fraction, frac.	0.0095	0.1904	0.1142	0.1428	0.2761	0.1428	0.1242

2.2.2 Derivation of the Near-Well Permeability Perturbations and the Homogeneous Model

To analyse the effects of viscous fingering in the inter-well 2D fine models described in the previous section, it was necessary to artificially trigger the formation of fingers by adding dynamics to the flow. Some early studies have applied truncation and round-off errors to trigger the instability (Claridge, 1972; Peaceman & Rachford Jr., 1962). However, the application of this method has proven to be unsuccessful except in case with adverse viscosity ratios. More recently methods used to trigger are more reliable. The first approach involves the use of a finite-amplitude perturbation of the front at $t = 0$ with a homogeneous permeability field. In the second method, a random permeability field is created, and the flow instability is propagated in the porous media due to the permeability difference which causes variations in the flow velocities.

In this study, near-well permeability variations were applied to the grid blocks containing the injection well to perturb the system thereby seeding the formation of viscous fingers. The formation and the propagation of the fingers were driven by the mobility ratio between the injected gas and reservoir oil, and physical diffusion and dispersion (longitudinal) (Christie & Bond, 1987; Peters et al., 1984). The use of fine grids mitigated the effects of numerical dispersion and diffusion. As a result, the fingers formed are physical instabilities that occur naturally, but they are deterministic and uncontrollable. The numerical effects/ noise caused by the perturbation seeds the

fingers, but when they are generated, they are not numerically propagated. The approach for generating the permeability perturbations is described below. The permeability perturbation of each injection well grid cell (identified with index, k was calculated using the equation:

$$K_k = K_{(x,z)}(1 + c \times \beta_k) \quad (10)$$

where c is the perturbation multiplier, β_i is the permeability variation in cell block i , and $i = 25$. While the parameter β_i determines the setting of the near-well perturbations, the constant c controls the variation of permeability in the resulting perturbations. A higher value of c implies a higher variability in the permeability perturbations. It was expected that for a high value of c , the degree of finger formation and propagation across the model will be significantly higher. Three classes of this constant $c = 0.01, 0.1$ and 1.0 were examined.

A set of values of the parameter β_i represents a realisation of the perturbation which controls the variation of the perturbation. Three classes of this parameter representing three different realisations were assessed. They are normally distributed and had a mean of zero and a standard deviation of 1.0 from the average permeability in the homogeneous case ($k = 721$ mD), and they were represented by perturbation β_1, β_2 and β_3 , respectively. Therefore, the realisations were correlated in terms of level of variations but were spatially random. The sum of product $c \times \beta_i$ for each realisation was always equals to zero so that the mean permeability of each realisation was equal to the permeability value given in Table 1 ($k = 721$ mD).

By creating realisations of the perturbation that had different degrees of variation of permeability around the mean, we were able to include the effect of this variation on the formation and propagation of viscous fingers. We were also able to assess the minimum degree of perturbation required to seed unique fingers. This was to be applied in simulation of the miscible floods in the heterogeneous models. Figure 3 shows some examples of the distribution of the resulting permeability perturbations multipliers i.e. $(1 + c \times \beta_i)$ applied to the injection well cell for three sets of perturbation.

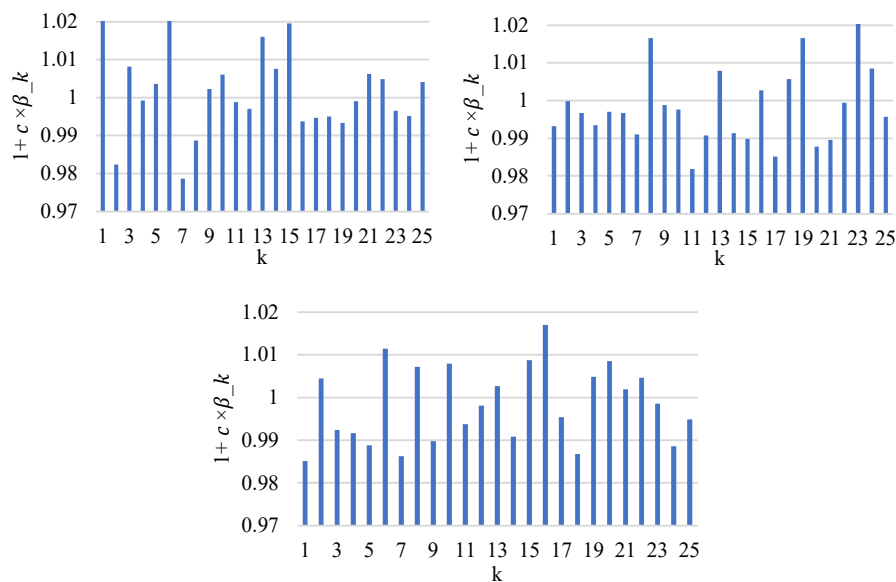


Figure 3: Histogram of the some resulting permeability perturbations multipliers i.e. $(1 + c \times \beta_i)$, applied to the injection well cell.

A displacement in a fully homogeneous reservoir (without near-well permeability perturbation) was also considered as a base case for comparison purposes. We applied these perturbations to the grid cells of the injection well in a fully homogeneous model and observed that the presence of these perturbations led to significant dissimilarities in the displacement process and in the overall performance of CO_2 flooding in the individual models. In contrast, the fluid production profiles and spatial distribution within the reservoir were unaffected by

the presence of the perturbations during the initial secondary waterflood process. This was due to the favourable mobility ratio between the injected water and reservoir oil which do not lead to the formation of fingers. Hence, in this chapter, we focused on the performance of the miscible gas flooding process.

2.2.3 Heterogeneous two-dimensional models

Here, we attempted to fully understand and quantify the effects of the interplay between the perturbations (viscous fingering) and reservoir heterogeneity in heterogeneous reservoir models and establish the levels of heterogeneity where flow will be defined by fingering versus the channelling. We did this by modelling simulation scenarios in which the permeability perturbations discussed in the previous section were applied to five-layered models with varying degrees of permeability heterogeneity (see Figure 4). While the near-well perturbations at $t_D=0$ artificially seeded and triggered the formation of viscous fingers, the presence of permeability variations propagated the fingers and, in some cases, led to the formation of thief zones or high permeable channels within the model depending on the level of heterogeneity. The descriptions of the permeabilities in the layers across the models generated are as presented in Figure 4.

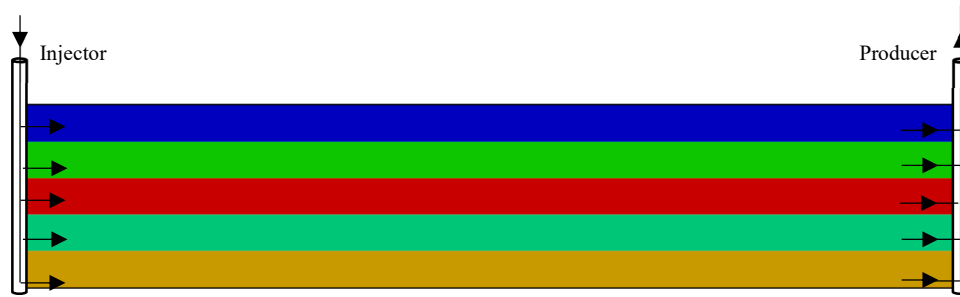


Figure 4: Representation of the five-layer model showing the placement of the injection and production wells.

The permeability of each layer (indexed as n) within a given permeability realisation is calculated using the equation:

$$K_n = K_{avg}(1 + K_{mult} \times \alpha_n) \quad (11)$$

where K_n is the permeability of layer n , K_{avg} is the average permeability (as given in Table 1), K_{mult} is the permeability multiplier and α_n is the permeability variation in layer n . Each layer is made of five grid cells in the vertical axis ($N_z = 5$), so that $n = 5$. α_n represents a realisation of global permeability which consists of a vector of 5 random numbers, which were generated for the distinct layers of the model shown in Figure 4 such that they were normally distributed, and they always had a zero mean, and a standard deviation of 1.0. Three sets of these vectors were created having the same means and standard deviations to represent the realisations of permeability realisations 1, 2 and 3 (i.e., α_1 , α_2 , and α_3). To generate 2D cross-sectional reservoir models with varying degrees of heterogeneity and scale the range of the permeabilities within each realisation, we applied four global permeability multipliers, $K_{mult} = 0.01, 0.25, 1.0$ and 1.50 to the α_n . The resulting models for any permeability realisation had the same average permeability, but different variations of permeability representing varying degrees of heterogeneity. As a result, the sum of product $K_{mult} \times \alpha_n$ for any realisation was always equal to zero. The histogram of the permeability distribution in the generated models is shown in Figure 5.

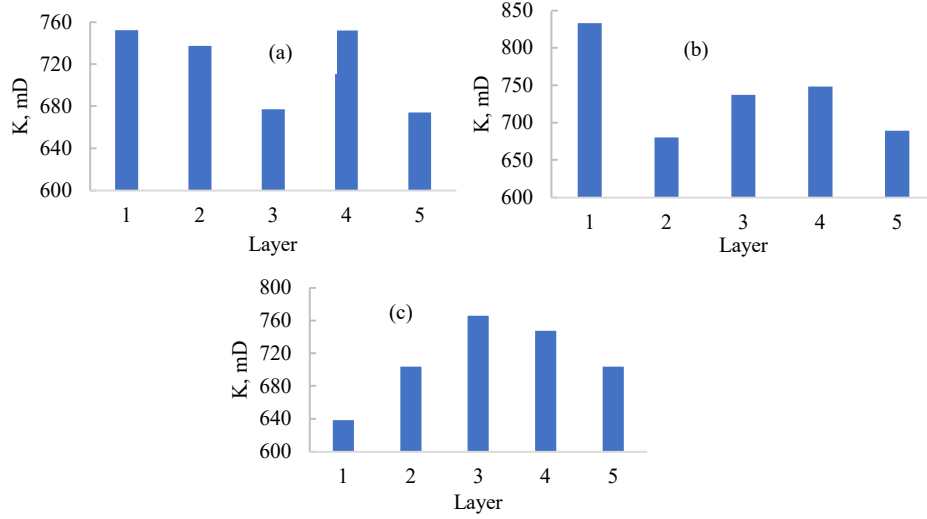


Figure 5: The distribution of the permeabilities in the five layers of the heterogeneous realisations (a) 1, (b) 2, and (c) 3, when $K_{mult} = 1.0$ was applied

In summary, the application of the multipliers (K_{mult}) to the permeability realisation increased the degree of permeability variation/heterogeneity within the realisation. Therefore, the realisations derived were correlated spatially with different levels of permeability variation within each realisation.

2.3 Dimensionless Scaling and Instability Analysis

To make the findings of this study transferable, we expressed the input data and results in forms of dimensionless number using quantities such as log viscosity ratio (R), Peclet number (Pe), dimensionless length, x_D , dimensionless time, t_D , (expressed as the pore-volume of gas injected), the mixing length, L_{mix} , etc. These equations are described below:

The mixing length, L_{mix} was used to express the spreading of the fingers across the reservoir and quantify the growth of the fingers. It is given as

$$L_{mix} = x_{c=0.12} - x_{c=0.98} \quad (12)$$

where $x_{c=0.12}$ and $x_{c=0.98}$ are the dimensionless distances ($x_D = x/L$) where the concentrations of CO_2 are 0.12 and 0.98 respectively.

The dimensionless time, t_D is given as the pore volumes injected (PVI) which is the ratio of the total injected volume to the reservoir's pore volume.

$$t_D = \frac{Qt}{\phi AL} \quad (13)$$

where A is the cross-sectional area of the reservoir, and t is time.

The Peclet number, Pe is given as:

$$Pe = \frac{UL}{D_L} \quad (14)$$

where D_L = longitudinal diffusivity (i.e., diffusion plus longitudinal dispersion), L is the length of the reservoir, U is the total flux of the fluid, and $R = \ln \left(M = \mu_g / \mu_o \right)$.

The interface between the injected and in-situ fluids is considered as unstable when $R > 0$, leading to complex fingering behaviour. The numerical simulations were carried out for an $R = 2.983$ suggesting that the flow was unstable. The Peclet number was calculated using the methods described by (Abdul Hamid & Muggeridge, 2020; Brock & Orr Jr., 1991; Perkins & Johnston, 1963). Based on the fluid flowrates and dimensions of the reservoir models applied, the Peclet numbers of the flow displacements in all the models studied was obtained as $Pe > 129$.

During miscible displacement, four fingering regimes are observed as the viscous fingers develop over time. They include the very early, early, intermediate and late time fingering regimes. The interested reader is referred to (Abdul Hamid & Muggeridge, 2020) for better explanation of this concept.

2.4 Linear Perturbation Analysis

In a homogeneous model, during the very early and early times of viscous fingering, the fingers grow linearly, and their behaviours can be described by the linear stability/perturbation theory presented by (Christie & Bond, 1987). This theory has also been applied in modelling viscous fingering in miscible floods by several authors (Abdul Hamid & Muggeridge, 2020; Jangir et al., 2022; Malhotra et al., 2015; Nijjer et al., 2018; Peaceman & Rachford Jr., 1962; Peters et al., 1984). In this study, we applied the theory to model the fingering behaviour and to predict the growth rates of the fingers during the miscible displacement. Using this method, it was possible to calculate the growth rates of the fingers as a function of dimensionless time, and also estimate the growth rates of the fingers and other relevant fingering parameters. According to (Christie & Bond, 1987) and (Tan & Homsy, 1986), there is a dimensionless finger wavenumber, k_m having a maximum dimensionless growth rate ω_m , and a cut-off wavelength k_c , so that flow at a wavelength less than the cut-off was considered as stable.

We analysed the fingering behaviour in the homogeneous model as a function of the mixing length, L_{mix} , finger growth rate (i.e., the mixing zone velocity), U_{mix} , a dimensionless finger wavenumber, k_m , maximum dimensionless growth rate ω_m , and the number of fingers vs. dimensionless time. From the linear perturbation theory, k_m and ω_m are given as (Abdul Hamid & Muggeridge, 2018; Tan & Homsy, 1986):

$$k_m = 0.118RPe, \quad (15)$$

and

$$\omega_m = 0.0225R^2 \quad (16)$$

The number of fingers, n_f can be estimated from the wavenumber by:

$$n_f = \frac{k_m}{2\pi} \quad (17)$$

The dynamics of fingering behaviour at the intermediate and late time fingering regimes cannot be explained using analytical solutions (Abdul Hamid & Muggeridge, 2020). Therefore, numerical simulations were instead applied to investigate this fingering behaviour on fine-scale grids models that minimised numerical diffusion.

3 Results and Discussion

In this section, the results of the homogeneous models to which the near-well perturbations were firstly presented and discussed. In the next section, we then present and discuss the results obtained for the heterogeneous stratified models.

3.1 Homogeneous Realisation with near-well perturbations

The multipliers, given by c were applied to the numbers derived when a standard deviation of 1% were applied to the permeability at the injection well. A displacement in the fully homogeneous reservoir case without perturbation was also considered as a base case for comparison purposes.

Figure 6 shows the distribution of CO₂ composition in the reservoir after 0.15 PV of gas injected. In the completely homogeneous model (the top model), viscous fingers that formed naturally were observed. These were formed due to the presence of an initial concentration difference between the injected solvent and oil where a reduction in dispersion resulted in the spreading of the interface in the direction of flow. Numerous studies on the numerical simulation of viscous fingering such as those by (Christie et al., 1993; Peaceman & Rachford Jr., 1962; Tan & Homsy, 1986; Tehelepi & Orr, 1994; Zimmerman & Homsy, 1991, 1992) amongst others have shown that

viscous fingers with small widths will form naturally whenever the Peclet number is sufficiently large as those observed in this study. At earlier times than this (i.e., the very early fingering time), the flow was controlled by the diffusion and a more stable front was observed i.e., little or no viscous fingers were formed. At this time, the onset of fingering was delayed in the fully homogeneous model because of the relatively higher magnitude of longitudinal dispersion. Here, fingering only begins to occur when there is a transition from a diffusive-dominated to a viscous-dominated flow.

In other models, fingering behaviours different from the non-perturbed case were observed due to the combined effects of lower dispersion and the perturbation at $t = 0$. As we will show later, the inclusion of different and increasing values of c was analogous to the application of different mobility values to artificially seed the formation of different fingers. As usual, the higher the mobility ratio of the fluids, or the higher the values of c , the more pronounced the fingering behaviour observed at the early time fingering regime is expected to be (Peters et al., 1984). Thus, the fingering behaviour in these models were more pronounced and there was more spreading of the fingers for the case where perturbation variability was at its maximum (when $c = 1.00$) signifying that there was a relationship between the degree of variation in the permeability perturbation and the length of the fingers or the fingering behaviour within the reservoir.

The study by [33] observed that there is a relationship between R and Pe , and the transition of the flow from the diffusive-dominated at the early-time fingering regime to viscous-dominated. For a given Pe , the crossflow from diffusion to fingering was earlier for a higher R . Since the use of near-well perturbations was done to mirror the inclusion of different mobility ratios, a higher value of c means a relatively higher of M and R . This implies that for a higher value of c , an earlier onset of fingering is expected as observed in the plots of Figure 6.

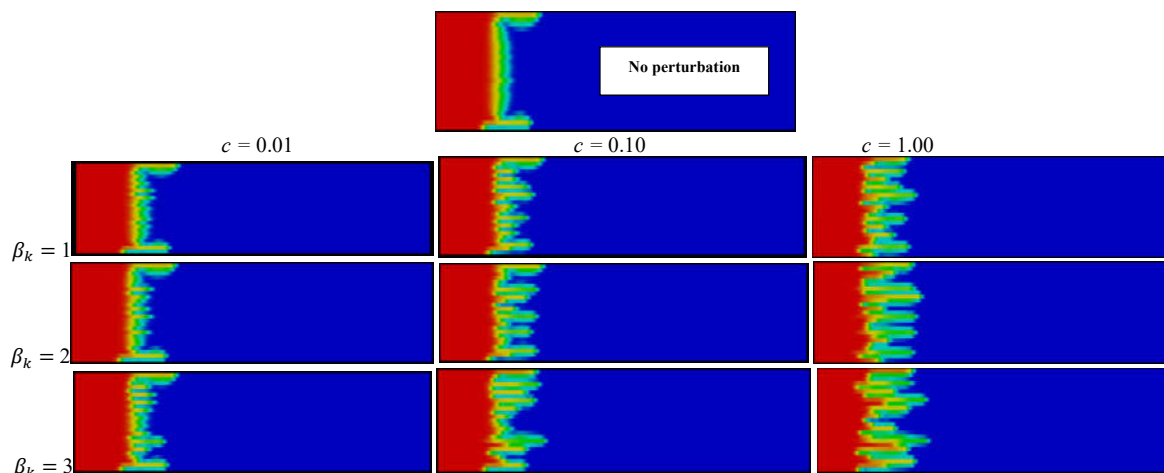


Figure 6: CO₂ concentration distribution at 0.15 PV of gas injected along the reservoir models for the homogeneous model (top), and the near-well perturbed models.

In summary, at the early time regime, the fingers are linearly unstable and grow exponentially particularly as the value of c increases, with the mixing zone growing diffusively. (Christie & Bond, 1987) suggested that linear stability analysis can be applied to predict the fingering behaviours of the perturbed reservoir models for short times i.e., the very early and early time fingering regimes. Using this theory, we described the behaviour of the fingers at the early time as described in Section 2.2 and shown below.

The spreading and growth of the mixing zone of unstable miscible displacements in homogeneous media can be modelled based on the prediction of (Koval, 1963) as cited by (Malhotra et al., 2015). Using this model, the mixing zone velocity can be computed as:

$$\frac{\Delta x}{t} = U \left(M_e - \frac{1}{M_e} \right) \quad (18)$$

The dimensionless frontal velocity, $U_{mix,D}$ is calculated by dividing the mixing zone velocity ($\frac{\Delta x}{t}$) by the total flux (U). Experiments by [35] suggested that the effective mobility ratio M_e can be calculated as:

$$M_e = (0.22M^{\frac{1}{4}} + 0.78)^4 \quad (19)$$

This equation has also been validated using numerical simulations (Booth, 2010; Tan & Homsy, 1986) and using fluid displacement experiments (Tchelepi et al., 1993).

Using these equations, we estimated the quantities from the linear perturbation theory, particularly the number of fingers and compared the values calculated analytically to those obtained from the numerical simulation, all at $t_D = 0.20$. Having calculated the dimensionless mixing zone velocity, $U_{mix,D}$, we applied Equation 9 to calculate the effective mobility ratio, and ‘pseudo’ mobility ratio of the perturbed systems. By doing this, we are able to mirror the mobility ratio of the perturbed systems and apply the linear perturbation theory to model the relevant dynamics of viscous fingering. Table 4 below shows the results obtained from this analysis. It shows a comparison of results from the linear perturbation theory to those obtained from numerical simulations at $t_D = 0.20$. As earlier described, across the three realisations, $\beta_k = 1, 2, \text{ and } 3$, it is seen that the values of the mixing length, mixing zone velocity, and the mobility ratios increased as the values of c increased from 0.01 to 1.0, meaning that there is a proportional relationship between the multiplier, c and the mobility ratio, M . Table 4 presents the results from the linear perturbation theory in comparison to those obtained from numerical simulations.

It is clearly seen from Table 4 that the fingering parameters estimated by the linear perturbation theory were in close agreement with the observations derived from the numerical simulations. For example, the number of viscous fingers estimated by the linear perturbation theory is similar to the number of fingers observed from the numerical simulation. Also, the mobility ratio estimated analytically is very close to the value applied in the numerical simulation when $M = 19.75$) Therefore, it can be said that the linear perturbation theory can be applied to predict the fingering behaviour of the perturbed homogeneous systems at very early, and early fingering times.

At intermediate fingering regime, i.e., 0.425 PV of gas injected (see Figure 7), a reduction in the number of fingers in each model is observed. This was because the fingers have attained a certain amplitude causing them to begin interacting with one another resulting in fingering coarsening/coalescence transversely, and finger growth longitudinally. At this time, the fingering fronts had progressed down the porous media and non-linear effects caused the finger to merge as seen in all models. As a result, this observed fingering pattern cannot be modelled using the linear stability theory. Also observed at time is that there is a general similarity in the characteristics of the fingers formed in all the model because of the physical mechanisms that act after the initiation of fingering at the early-time fingering regime. Therefore, at this regime, the fluid flow was dominated by these non-linear finger interactions/ mechanisms.

Table 4: A comparison of results from the linear perturbation theory to those obtained from numerical simulations.

	No Pert	$\beta_k = 1$			$\beta_k = 2$			$\beta_k = 3$		
		c=0.01	c=0.1	c=1.0	c=0.01	c=0.1	c=1.0	c=0.01	c=0.1	c=1.0
$L_{mix,D}$	0.49	0.48	0.49	0.63	0.49	0.54	0.58	0.52	0.59	0.62
$U_{mix,D}$	1.96	1.92	2.12	2.62	1.93	2.41	2.59	2.18	2.66	2.7
M_e	2.38	2.35	2.52	2.96	2.36	2.77	2.93	2.57	2.99	3.03
M	19.45	18.77	22.61	34.05	19	28.95	33.17	23.78	35.07	36.13
R	2.97	2.93	3.12	3.53	2.94	3.37	3.5	3.17	3.56	3.59
k_m	50.9	50.47	49.41	57.44	51.14	51.24	53.92	51.53	54.29	57.72
ω_m	0.2	0.19	0.22	0.28	0.2	0.25	0.28	0.23	0.28	0.29

Pe_L	145.4	144.88	134.68	137.97	147.19	129.02	130.5	137.83	129.32	136.37
n_f (Analytical)	8.1	8.03	7.86	9.14	8.14	8.15	8.58	8.2	8.64	9.19
n_f (Simulation)	8	8	8	9	8	8	8	8	8	9

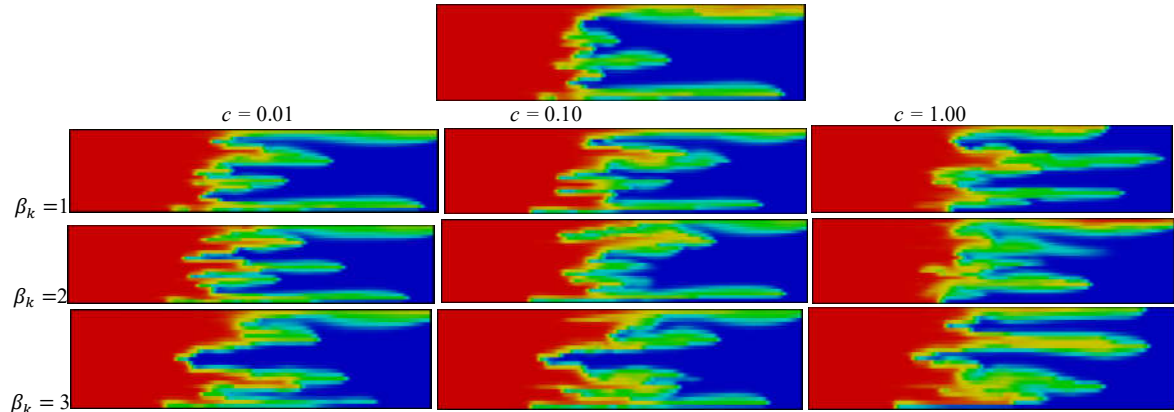


Figure 7: CO₂ concentration distribution at 0.425PV of gas injected along the reservoir models for the homogeneous model (topmost), and the perturbation models.

At 0.85 PV of gas injected (Figure 8), further merging of the fingers had occurred in all the cases as the fingers migrated towards the production wells, and this was observed to be the predominant method of finger growth. At this time, the flow is composed of exponentially slowing, finger exchange flow, and diffusion in the direction of the flow dominates the dynamics of the process irrespective of the magnitude of the perturbation (or mobility ratio) applied to seed the fingers.

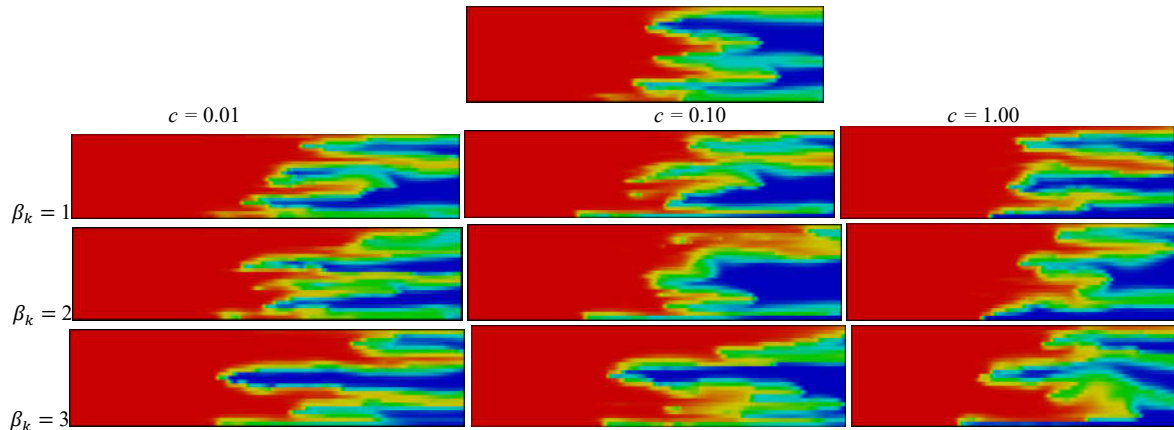
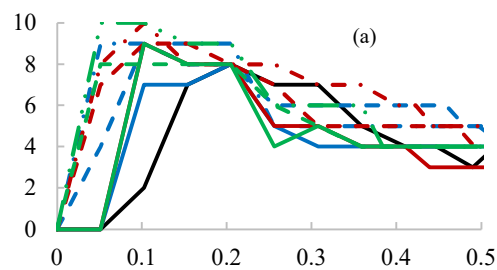


Figure 8: CO₂ concentration distribution at 0.85PV of gas injected along the reservoir models.

Figure 9 shows the growth and decay of the fingers, represented by the number of fingers, n_f vs. dimensionless time, t_D , throughout the numerical simulation. Figure 9 (a) shows this growth and decay during the very-early, early and intermediate fingering regimes. At the very early time, there were no fingers formed due to stability of the mixing front imposed by the molecular diffusion, and $n_f \sim 0$. It was observed that the formation of fingers was delayed in the fully homogeneous model and in the models of $c = 0.01$ during the early fingering time. As earlier described, this was so because the low value of c applied led to a reduction in the mobility ratio, and hence a delay in the onset of finger formation.



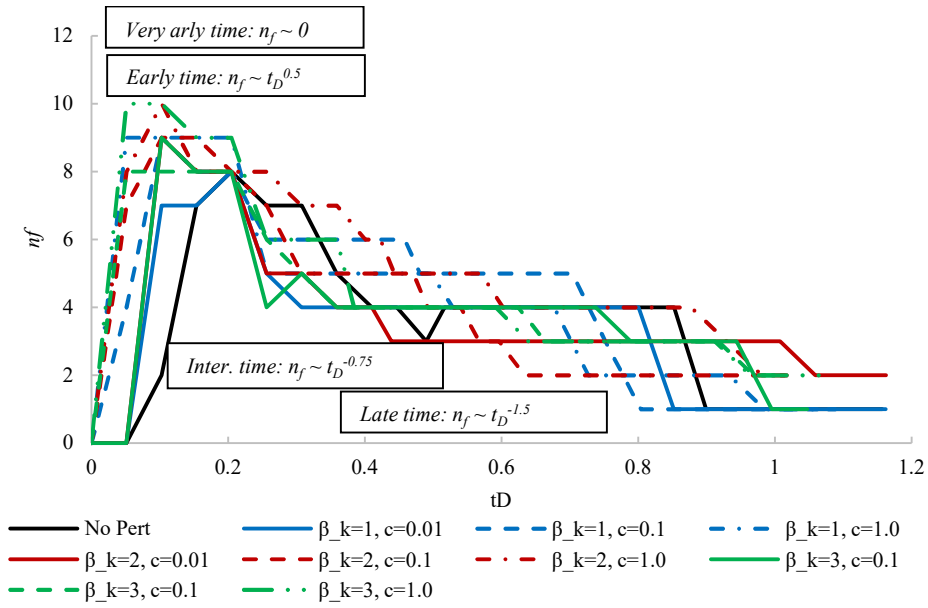


Figure 9: The growth and decay of the fingers vs. dimensionless time at the end of the numerical simulation. The inset figure (Figure (a)) shows the growth and decay during the very-early, early and intermediate fingering regimes.

In all the models, after the formation of the fingers, its number then increased sharply to their maximum values during the early fingering regime, and then began to decay afterwards (during intermediate time, after $t_D > 0.20$) largely due to fingering coalescence/ merging. Around $t_D = 0.25$, the number of fingers in the model having $\beta_k = 3$ and $c = 0.01$ was observed to increase from 4 to 5 as a result of a fingertip splitting event that occurred in the leading finger. Afterwards, all the models experience a steady decay in numbers of fingers observed due to the continuous finger merging culminating in one or two fingers at the end of the simulation (late fingering time).

The relationship between the number of fingers formed as a function of dimensionless time is also presented in Figure 9. This relationship was computed by averaging the number of the fingers formed in all models at each time considered. It shows that the number of fingers grow proportionally at $n_f \sim t_D^{0.5}$ during the very early, and early fingering regimes after which they begin to decay. At the intermediate fingering and late time regimes, the number of fingers decays monotonously at $n_f \sim t_D^{-0.75}$, and $n_f \sim t_D^{-1.5}$, respectively due to further merging of the fingers.

In conclusion, the results of the homogeneous models have shown the applicability of the linear stability theory to analytically model the fingering behaviour and reproduce the results predicted by the numerical simulation, during the very early and early time fingering regimes. For the range of permeability heterogeneity applied in this model, (i.e. when heterogeneity = 0), the viscous fingers which were either formed naturally or artificially triggered by the perturbations/ noise applied at $t_D = 0$, play a dominant role in finger formation and growth at the very early and early times fingering regimes. As the displacement progresses towards the intermediate and late fingering times, the influence of the viscous fingering diminishes and physical diffusion in the predominant direction of flow dominated the process.

Figures 10 and 11 show the gas and oil production profiles of the homogeneous models, respectively. Using the oil and gas production rates, the influence of the fingering behaviours on the performances of the different models of the miscible flooding process can be shown. Since the objectives of a miscible CO_2 injection was to improve oil recovery, and store the injected gas in the subsurface porous media, it was necessary to assess the effects of the fingering behaviour on these objectives. The use of the concentration and saturation maps alone does not adequately present this assessment.

From the production profiles, it was observed that they were dissimilarities of the fluid production profiles for each model throughout the miscible flooding period. This was because the addition of the near-well perturbations of different characteristics led to different fluid production rates as was observed for the saturation/ concentration plots (Figs. 6 – 9).

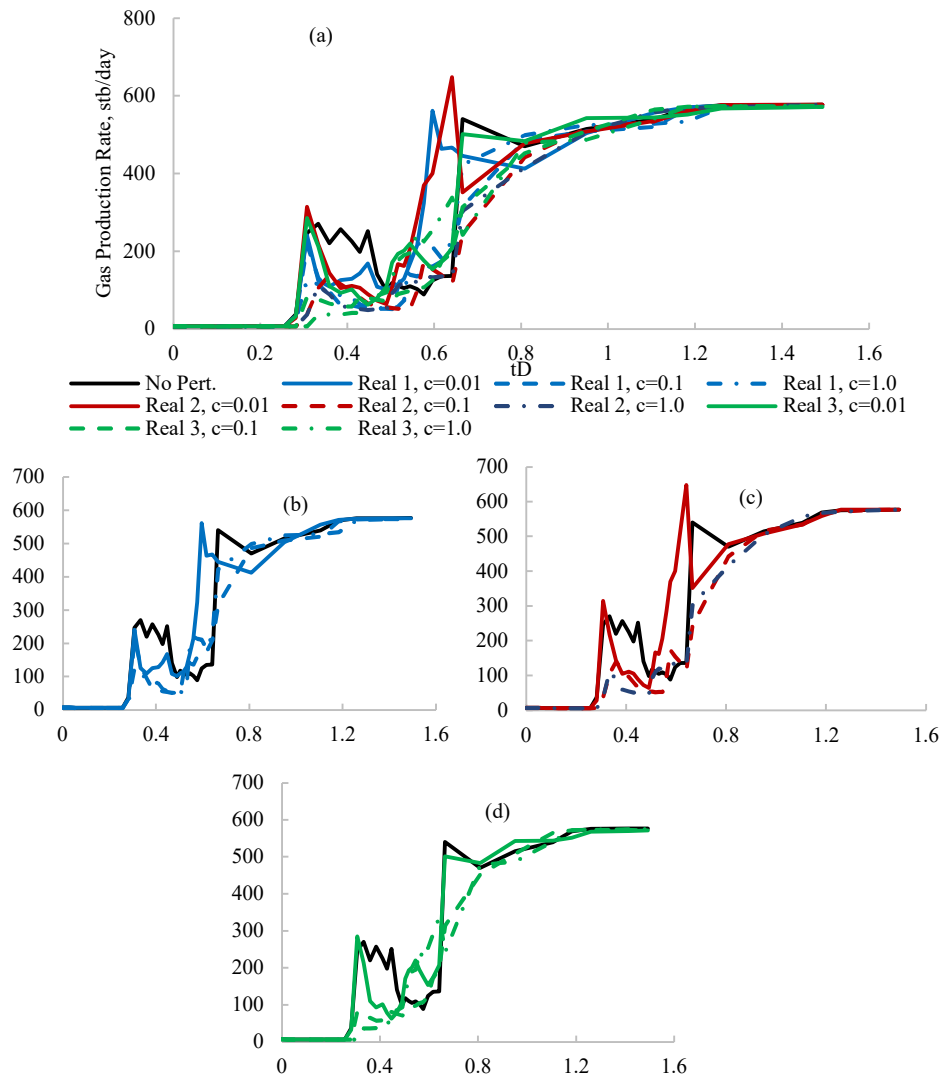
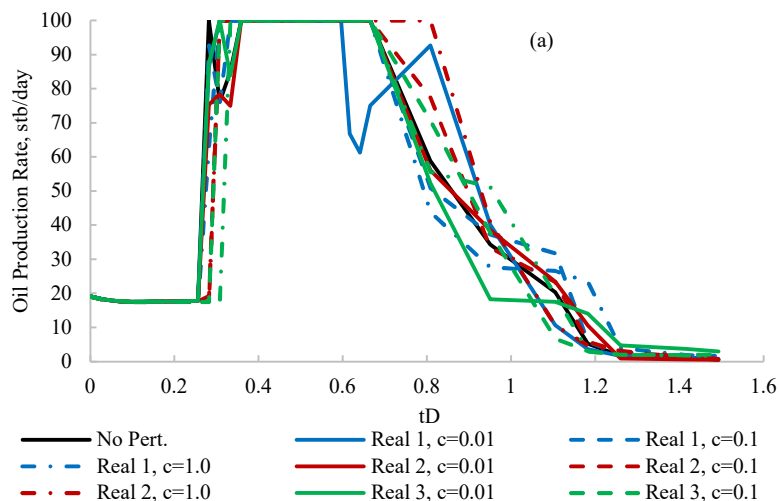


Figure 10: (a) Gas production rate versus time of the models in the homogeneous case. The smaller sub-plots show the gas production rates of the no-perturbation case, and cases of the (b) realisation 1, (c) realisation 2, and (d) realisation 3, shown for the different values of c .



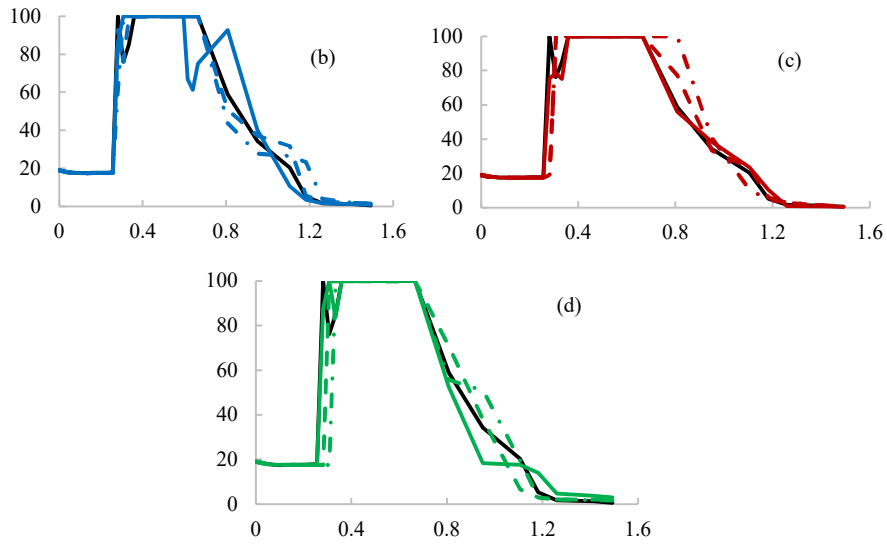


Figure 11: (a) Oil production rate vs. time of the models in the homogeneous case. As usual, the smaller sub-plots show the gas production rates of the non-perturbed case, and cases of the (b) realisation 1, (c) realisation 2 and (d) realisation 3, shown for the different values of c .

To compare the differences between the production profiles discussed, we then calculated the similarities of the profiles of each model (taken as the dependent variable) to every other model (the covariates) using a multivariate regression analysis or R-squared. This was given as the average of the correlations of the oil and gas production rates. We then derived a covariance matrix of this similarities as presented in Table 5 below. Using a scale of 0 – 1, a value of R-squared close to 0 implies little correlation, while a value of 1 means perfect similarity between models. The models with the same realisation of perturbation are grouped together with borders around their values as shown

Table 5: Correlation Matrix of the R-squared values of the (a) gas, and (b) oil production rates of the models explored in the fully homogeneous case.

		No Pert	$\beta_k=1$			$\beta_k=2$			$\beta_k=3$		
			c = 0.01	c = 0.1	c = 1	c = 0.01	c = 0.1	c = 1	c = 0.01	c = 0.1	c = 1
	No Pert	1.00									
$\beta_k=1$	c = 0.01	0.89	1.00								
	c = 0.1	0.97	0.92	1.00	0.98						
	c = 1	0.95	0.93	0.98	1.00						
$\beta_k=2$	c = 0.01	0.89	0.95	0.94	0.94	1.00					
	c = 0.1	0.93	0.90	0.96	0.97	0.90	1.00	0.99			
	c = 1	0.92	0.90	0.95	0.96	0.89	0.99	1.00			
$\beta_k=3$	c = 0.01	0.97	0.92	0.98	0.98	0.93	0.94	0.95	1.00		
	c = 0.1	0.93	0.91	0.96	0.97	0.91	0.99	0.99	0.95	1.00	0.95
	c = 1	0.88	0.89	0.94	0.94	0.92	0.94	0.94	0.91	0.95	1.00

As seen from the table (Tables 5), there was a varying level of similarity in the trends observed between the gas and oil production profiles in any of the model meaning that even a small amount of perturbation applied to the homogeneous model can cause differences in the behaviour of fluid flow in the system and its production from the oil well. In the absence of the perturbations, the value of R-squared would be equal to 1. Overall, the results show that the models are quite similar to one another with R-squared values varying from 0.88 to 1.0. Generally, the results obtained for models of the same realisation, β_k showed more similarities to each other than they do to the models of other realisation.

Based on the results obtained from the application of the perturbations to the homogeneous model, we can conclude that the presence of the perturbations (or different mobility ratio) causes significant changes in the

dynamics of the miscible displacement process. Also, at this level of reservoir heterogeneity (heterogeneity = 0), the flow of the injected gas at the early fingering time was dominated by the difference of viscosity between the injected and the resident fluids which leads to the formation of viscous fingers. However, as the fingers travel through the porous media, the influence of the viscous fingers waned, and fluid flow was dominated by physical or molecular diffusion.

3.2 The Stratified Models (The Heterogeneous Permeability Realisations)

In this section, we present and discuss the results obtained when the perturbations are applied to the first realisation of the stratified models. To quantify the effects of heterogeneity and viscous fingering, we considered the numerical simulation of the miscible CO₂ flood in the realisation of heterogeneous permeability (described as vectors of α_n). Based on results from study of the homogeneous model (Section 3.1), we observed that a very small degree of perturbation can artificially trigger different fingering behaviours in the porous media. Here, we present a comparison of the flow visualisations and the performances of the dynamic process. We first quantified the interplay of viscous fingering and channelling in CO₂ flooding by modelling the process using a realisation of the global permeability. To vary the strength of the artificial viscous fingers, we applied three levels of the perturbations variability represented by c . As seen from the linear perturbation analysis of the previous section, this is analogous to the varying the mobility ratio between the injected and in-situ fluids. Finally, in the concluding section, we assessed these effects in the three global realisations of permeability. Here, we applied the three levels/realisations of the near-well perturbations and the lowest multiplier, $c = 0.01$, to the heterogeneous models.

3.2.1 Quantifying the interplay of viscous fingering and channelling in CO₂ flooding processes

Figure 12 shows the CO₂ concentration distribution at 0.15PV of gas injected along the heterogeneous permeability models. When $K_{mult} = 0.01$, the relatively low value of the multiplier applied to the permeability realisation reduced the degree of heterogeneity in the models and the injected gas may finger through the model because of viscosity contrast, and not because of the presence of heterogeneity. The number of fingers formed decreased as the value of the permeability multiplier (K_{mult}) applied increased, and that the distance travelled by the fingers i.e., the mixing length was greater as K_{mult} increased for any given value of c . The formation of the fingers was more pronounced (i.e., more fingers were formed) for the cases where K_{mult} is low.

The trends of CO₂ distribution in the models with the same K_{mult} were very similar particularly when $c = 0.01$ and 0.1. However, when $c = 1.0$, a different trend was observed particularly for the low values of K_{mult} , i.e., $K_{mult} = 0.01$ and 0.25 which can be attributed to the large variation in the strength of the perturbation imposed by the relatively higher value of c which ensured that the flow behaviour was dominated by the artificially viscous fingers, particularly when K_{mult} is low (i.e., the models are fairly homogeneous).

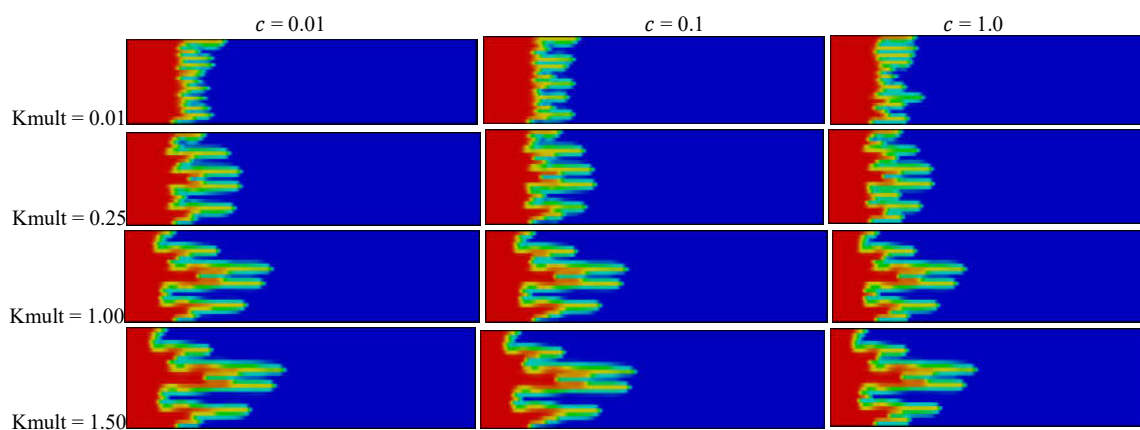


Figure 12: CO₂ concentration distribution at 0.15PV of gas injected along the reservoir models for the reservoir models of permeability realisation 3.

When $K_{mult} = 0.01$, the concentration plots for any value of c were different going from left to right irrespective of the strength of the perturbation. This was because the amount of heterogeneity included at this level was insufficient to dominate fingering, and viscous effects dominated at this stage. However, when $K_{mult} = 1.00$ and 1.50 , the concentration plots looked similar for each value of c and the effects of the high permeability zones in layers 3 and 5 were prominent as the injected gas began to propagate/channel through these layers. Therefore, the amount of heterogeneity induced in these models by the permeability multipliers was sufficient to influence the propagation of the injected gas in the porous media, and permeability heterogeneity dominates flow of fluids. In the layered streak models, most of the flow occurred in the higher permeability layers which were wide enough for the viscous fingers to form and grow within them. This trend was observed when $K_{mult} = 0.25$, 1.0 and 1.50 .

Figure 13 shows the distribution plot of CO₂ concentration at 0.425PV of gas injected. In the first row, that the distribution of CO₂ concentration was observed to be different with value of c as value of permeability multiplier applied in this case was very low and this effect reduced the amount of heterogeneity in the model. As a result, viscous fingering induced by the perturbations continues to control the dynamics of the process. Thus, no common trend/pattern is observed in the distribution plots of CO₂ concentration when $K_{mult} = 0.01$.

However, some similarity of the trend of fingering for each perturbation was observed in the other permeability multipliers particularly when $K_{mult} = 1.00$ and 1.50 which was very prominent. Also, the gas channelled through the high permeability layers and reaches at the production well, clearly avoiding the low permeability layer at the top of the reservoir.

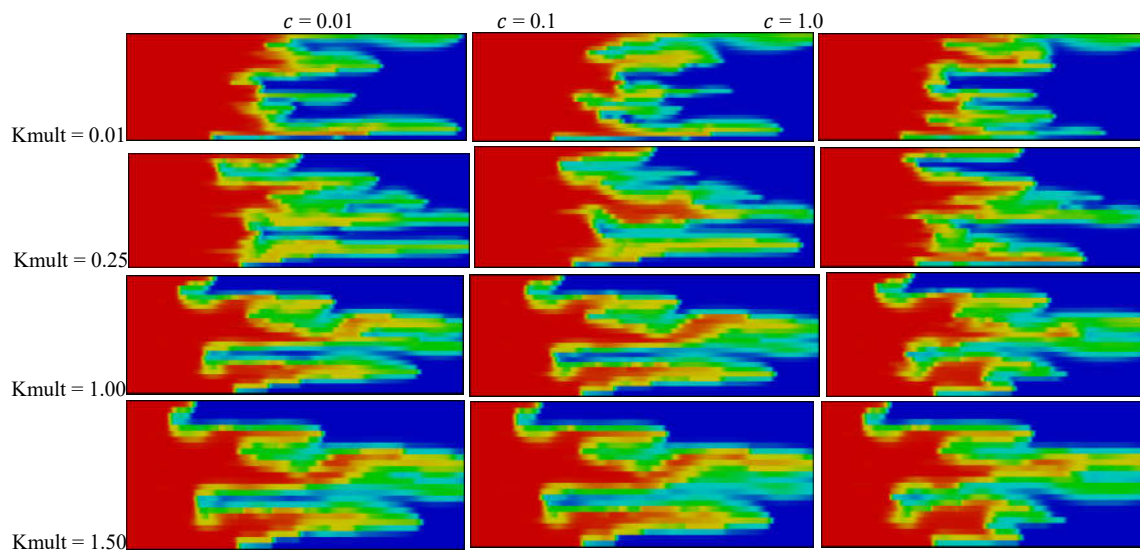


Figure 13: CO₂ concentration distribution at 0.425PV of gas injected for the reservoir models of heterogeneous permeability realisation 3.

At 0.85 PVI (see Figure 14), there was no similarity in the fingering trends observed in the concentration distribution maps for any of the models derived using $K_{mult} = 0.01$ and 0.25 . This means that viscous fingering forces still exhibit a dominant effect over the displacement process particularly in the first permeability multiplier case while a combination of viscosity-induced fingering and heterogeneity-influenced channelling dominates when $K_{mult} = 0.25$.

When $K_{mult} = 1.00$ and 1.50 , the application of the first and second values of c resulted similarities in the spatial distribution of CO₂ meaning that in these cases, permeability heterogeneity/ channelling exerted a dominant effect on the performance of the process. However, this behaviour was not observed when $c = 1.0$. In

both cases of K_{mult} , the use of $c = 1.0$ resulted in different spatial distributions of the injected gas. Therefore, it can be said for these cases that the strength/setting of the perturbation or noise imposed in this case was large enough so that even though reservoir heterogeneity was significant, the viscous fingers induced by $c = 1.0$ still exerted a dominant influence on the miscible displacement process in the porous media. Hence, in these models, a combination of viscous forces, physical diffusion, and heterogeneity dominated the fluid flow as channelling and viscous fingering. This implies that during miscible floods where the viscosity or mobility contrast between the resident and injected fluids is relatively large, the effect of the resulting viscous fingers would be prominent irrespective of the level of heterogeneity of the porous media. Generally, for these cases of permeability multipliers, there were areas of the reservoir which were unswept by the injected gas, particularly at the top of the reservoir (the low permeability layer).

In conclusion, in the heterogeneous permeability models, the application of different K_{mult} 's to the different scenarios caused the reservoir's permeability to contain some level of heterogeneity. Therefore, a combination of viscous/diffusive forces and heterogeneity or just heterogeneity alone may control the flow displacement and performance of the CO_2 flood depending on the level of heterogeneity and/or the viscosity contrast/mobility ratio.

The evolution of the number of fingers in the heterogeneous models with dimensionless time is shown in Figure 15. The inset figures (Figure 15 (b) – (e)) show the growth and decay of the fingers for the models formed using the different K_{mult} 's. The growth of the fingers during the early time regime, and their subsequent decay during the late-time fingering regime was observed in all, the models. The fingering behaviour of the models formed when $K_{mult} = 0.01$ were similar to those observed in the homogeneous model seen earlier. As earlier discussed, this trend can be attributed to the low amount of heterogeneity imposed on the system by this low value of K_{mult} .

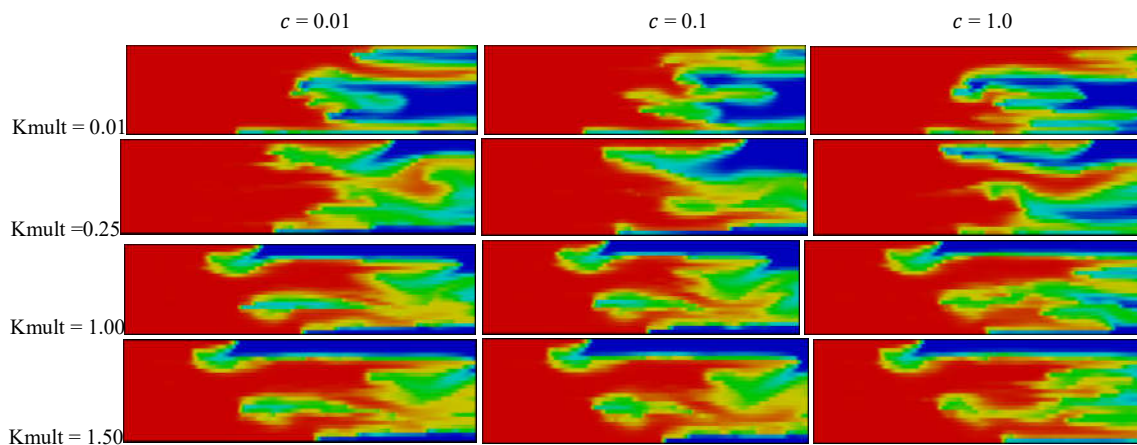


Figure 14: CO_2 concentration distribution at 0.85PV of gas injected along the reservoir models for the reservoir models of permeability realisation 3.

Overall, the maximum number of fingers formed was 10 when $K_{mult}=0.01$, 9 when $K_{mult}=0.25$, 7 when $K_{mult}=1.0$, and 5 when $K_{mult}=1.50$, implying more adverse fingering behaviour as the value of K_{mult} increases. Also observed was that as the value of K_{mult} increased, there was more similarity between the models of the same permeability multiplier, particularly when $c = 0.01$, and 0.1. For example, the evolution of the fingers with time observed when $K_{mult} = 1.0$ and 1.50 were perfectly similar and matched each other which implies that the displacement in these models was totally dominated by the channelling due to permeability variation or heterogeneity.

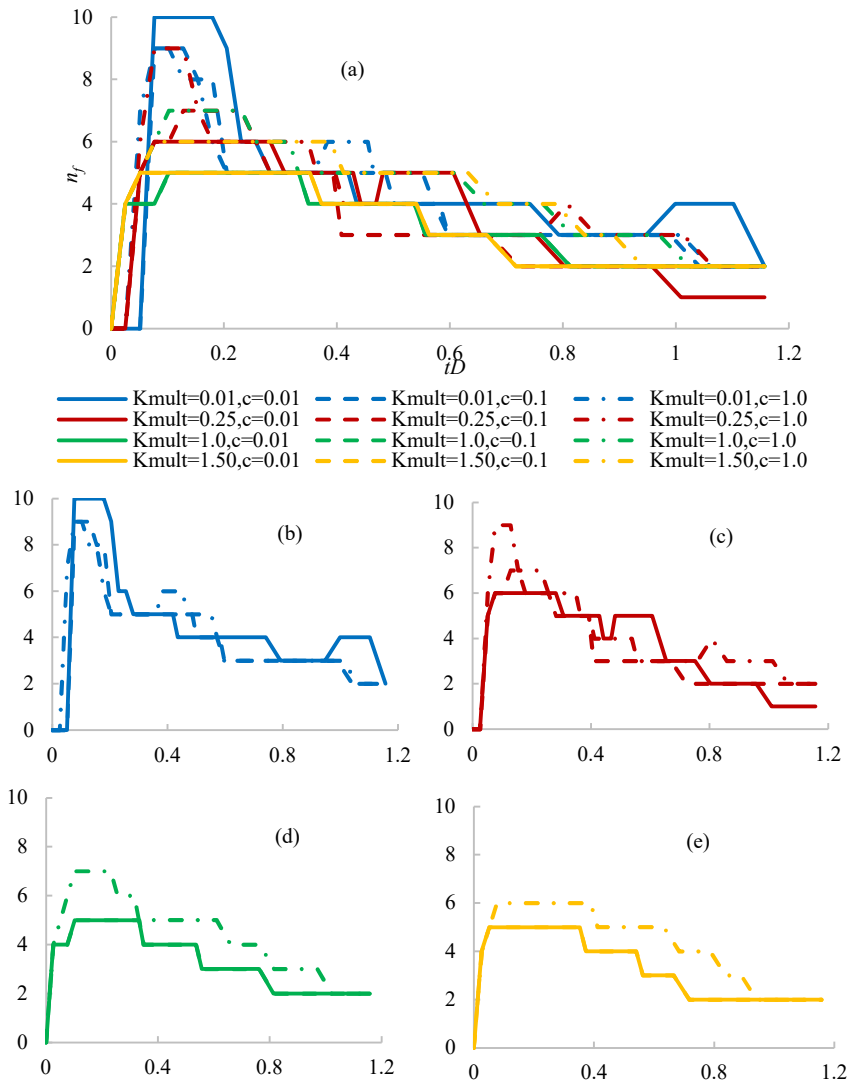


Figure 15: The growth and decay of the fingers vs. dimensionless time at the end of the numerical simulation. The inset figures (Figure 15 (b) – (e)) show the growth and decay during the very-early, early and intermediate fingering regimes.

However, the application of $c = 1.0$ to the models of $K_{mult} = 1.0$ and 1.50 did not follow the trends observed when $c = 0.01$ and 0.1 were applied as there were deviations in the number of fingers with time in both models. As earlier advised, this was because the use of this value of c resulted in more variability in the setting of perturbation imposed on the heterogeneous reservoir so that in these cases, viscous fingering/diffusion induced by this level of noise still exerted a significant influence on the performance of the displacement process. Figures 16 and 17 show the gas and oil production profiles of the models in realisation 3, respectively.

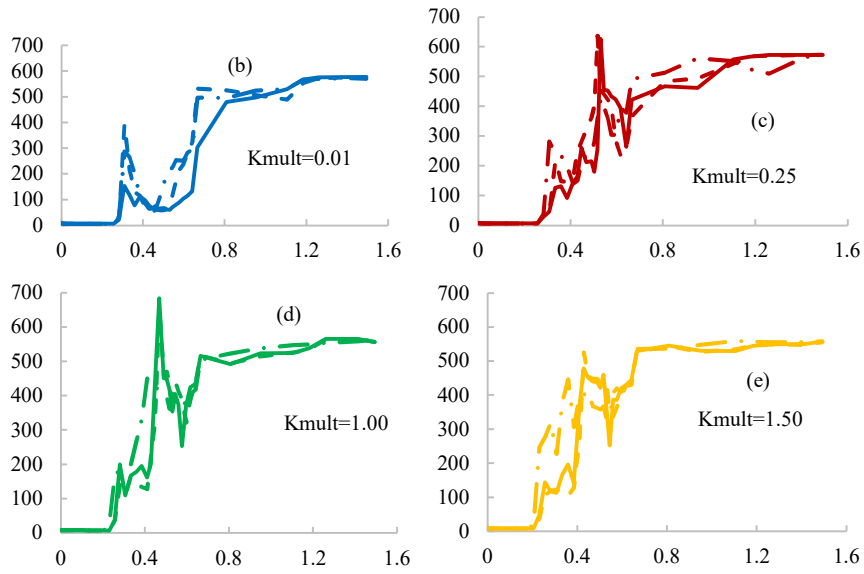
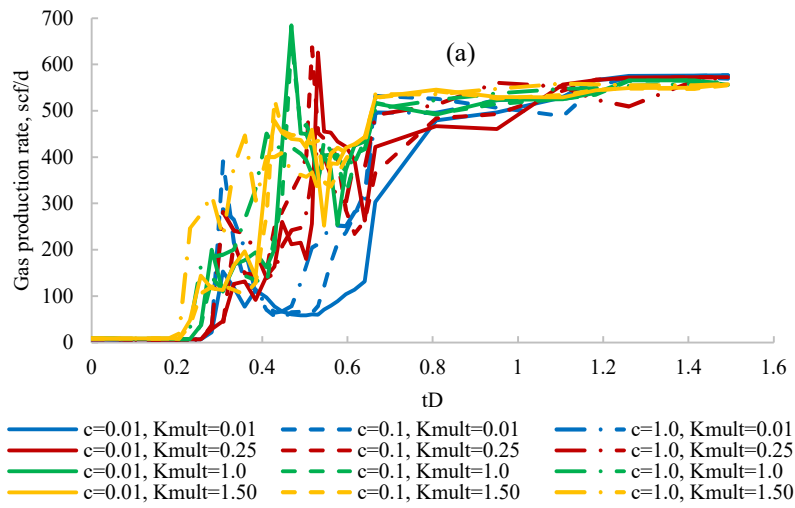
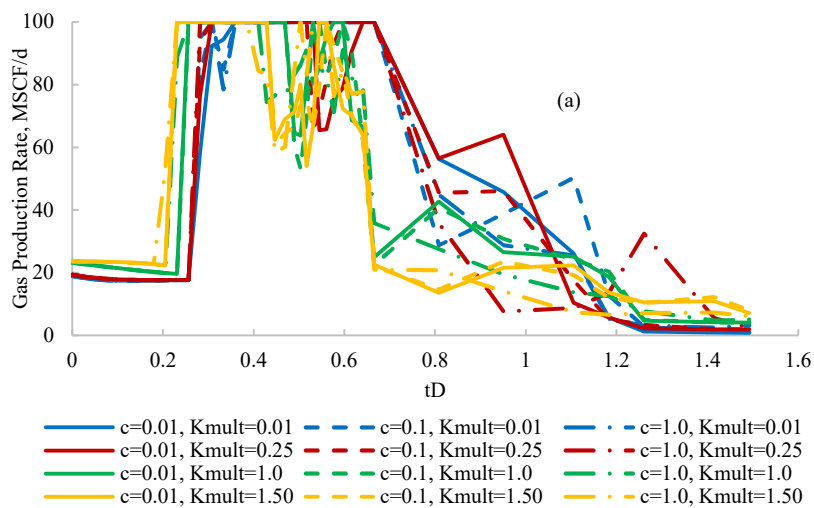


Figure 16: (a) Gas production rate versus time of the models of the Realisation 3. The inset sub-plots show the production rates of the cases where (b) $K_{mult} = 0.01$, (c) $K_{mult} = 0.1$, (d) $K_{mult} = 1.0$, and (e) $K_{mult} = 1.50$



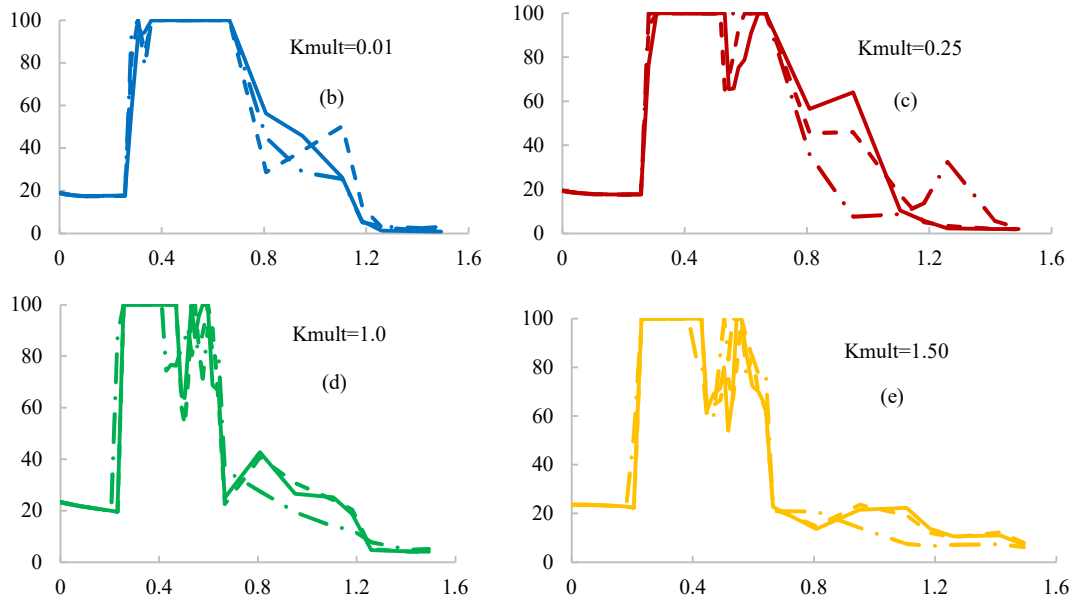


Figure 17: (a) Gas production rate versus time of the models of heterogeneous permeability. The smaller sub-plots show the production rates of the cases where (b) $K_{mult} = 0.01$, (c) $K_{mult} = 0.1$, (d) $K_{mult} = 1.0$, and (e) $K_{mult} = 1.50$. The legends are shown in Figure 16(a)

Table 6: Correlation Matrix of the R-squared values of the (a) gas, and (b) oil production rates, of the models of heterogeneous permeability

		$K_{mult}=0.01$			$K_{mult}=0.25$			$K_{mult}=1.00$			$K_{mult}=1.50$		
		$c = 0.01$	$c = 0.1$	$c = 1.0$	$c = 0.01$	$c = 0.1$	$c = 1.0$	$c = 0.01$	$c = 0.1$	$c = 1.0$	$c = 0.01$	$c = 0.1$	$c = 1.0$
$K_{mult}=0.01$	$c = 0.01$	1.00											
	$c = 0.1$	0.90	1.00	0.90									
	$c = 1.0$	0.90	0.90	1.00									
$K_{mult}=0.25$	$c = 0.01$	0.85	0.85	0.90	1.00								
	$c = 0.1$	0.84	0.82	0.89	0.93	1.00	0.93						
	$c = 1.0$	0.89	0.92	0.96	0.92	0.93	1.00						
$K_{mult}=1.00$	$c = 0.01$	0.73	0.74	0.78	0.79	0.84	0.84	1.00					
	$c = 0.1$	0.72	0.74	0.78	0.80	0.85	0.84	0.98	1.00	0.93			
	$c = 1.0$	0.73	0.74	0.78	0.80	0.83	0.84	0.94	0.93	1.00			
$K_{mult}=1.50$	$c = 0.01$	0.67	0.69	0.72	0.73	0.78	0.78	0.88	0.88	0.95	1.00		
	$c = 0.1$	0.67	0.68	0.72	0.75	0.79	0.79	0.89	0.88	0.95	0.99	1.00	0.94
	$c = 1.0$	0.69	0.71	0.75	0.72	0.74	0.79	0.82	0.81	0.94	0.95	0.94	1.00

Table 6 shows the correlation matrix of the R-squared values of the models of the heterogeneous permeability models taken as the averages of the correlations (R-squared values) of the oil and gas production rates. Relatively lesser correlations or similarities were observed in the fluid production profiles of the models formed using $K_{mult} = 0.01$ and 0.25 . This is also proven by the correlation matrices (Table 6). For example, a correlation of $R^2 = 0.90$ was observed when $K_{mult} = 0.01$, and $R^2 = 0.92$ and 0.93 when $K_{mult} = 0.25$. This was because the degree of reservoir heterogeneity induced by these relatively low values of permeability multiplier was low, and the viscous fingering and diffusive forces still dominated the flow of the reservoir fluids.

When $K_{mult} = 1.00$ and 1.50 , the production profiles started to show some similarity, particularly when $c = 0.01$ and 0.1 . The R-squared values of the models having $c = 0.01$ and 0.1 , were approximately equal to each other because of the similarities in the fluid production rates as the production profiles were clearly seen to overlap each other, particularly in the scenarios where $K_{mult} = 1.50$. Therefore, in these cases, permeability heterogeneity exerted a dominant effect on the performance of the displacement process, and the effects of viscous fingering were very minimal or non-existent. This trend was not observed in the third set of perturbations (i.e., when $c = 1.0$) as the R-squared was observed to be further away from unity and not well correlated. However, the application of the near-well perturbations of $c = 1.0$ resulted in the some deviations of the production profiles.

In order to further understand these observed trends, we assessed the correlations of the fluid production rates obtained from the models formed using three different realisations of the heterogenous permeability denoted by $\alpha_n = 1, 2$ and 3. This was done for the different values of K_{mult} as shown in Table 7. Since the results obtained earlier showed that the presence of small near-well perturbations was sufficient to artificially trigger different types of viscous fingers, we applied the realisations of the near-well perturbations (β_k) when $c = 0.01$ which mean that the system would have the same “mobility ratio”. It should be noted that the models of a realisation of global permeability given by α_n had the same level of heterogeneity and that the differences in heterogeneity were only imposed on the porous media by applying the permeability multipliers, K_{mult} . Therefore, the models of $K_{mult} = 0.01$ were the least heterogeneous while those of $K_{mult} = 1.50$ were the most heterogeneous. Table 7 shows the correlation matrix of the R-squared values of the fluid production rates obtained for the models formed when $K_{mult} = 0.01, 0.25, 1.0$, and 1.50 .

Table 7: The correlation matrix of the R-squared values of the fluid production rates obtained for the models formed when $K_{mult} =$ (a) 0.01, (b) 0.25, (c) 1.0, and (d) 1.50.

		$\alpha_n=1$			$\alpha_n=2$			$\alpha_n=3$					$\alpha_n=1$			$\alpha_n=2$			$\alpha_n=3$													
		$\beta_k=1$	$\beta_k=2$	$\beta_k=3$	$\beta_k=1$	$\beta_k=2$	$\beta_k=3$	$\beta_k=1$	$\beta_k=2$	$\beta_k=3$			$\beta_k=1$	$\beta_k=2$	$\beta_k=3$	$\beta_k=1$	$\beta_k=2$	$\beta_k=3$	$\beta_k=1$	$\beta_k=2$	$\beta_k=3$											
$\alpha_n=1$	$\beta_k=1$	1.00									(a)	$\alpha_n=1$	$\beta_k=1$	1.00									(b)									
	$\beta_k=2$	0.91	1.00	0.97									$\beta_k=2$	0.89	1.00	0.94																
	$\beta_k=3$	0.92	0.97	1.00									$\beta_k=3$	0.96	0.94	1.00																
$\alpha_n=2$	$\beta_k=1$	0.93	0.97	0.97	1.00						$\alpha_n=2$	$\beta_k=1$	0.76	0.82	0.81	1.00						$\alpha_n=2$	$\beta_k=1$	0.76	0.82	0.81	1.00					
	$\beta_k=2$	0.94	0.98	0.97	0.98	1.00	0.98					$\beta_k=2$	0.79	0.83	0.84	0.94	1.00	0.92			$\beta_k=2$		0.79	0.83	0.84	0.94	1.00	0.92				
	$\beta_k=3$	0.92	0.99	0.99	0.98	0.98	1.00					$\beta_k=3$	0.71	0.78	0.77	0.98	0.92	1.00			$\beta_k=3$		0.71	0.78	0.77	0.98	0.92	1.00				
$\alpha_n=3$	$\beta_k=1$	0.98	0.92	0.95	0.94	0.95	0.94	1.00			$\alpha_n=3$	$\beta_k=1$	0.87	0.94	0.91	0.87	0.88	0.84	1.00			$\alpha_n=3$	$\beta_k=1$	0.87	0.94	0.91	0.87	0.88	0.84	1.00		
	$\beta_k=2$	0.94	0.97	0.97	0.97	0.97	0.98	0.95	1.00	0.97		$\beta_k=2$	0.89	0.94	0.93	0.80	0.85	0.76	0.95	1.00	0.94		$\beta_k=2$	0.89	0.94	0.93	0.80	0.85	0.76	0.95	1.00	0.94
	$\beta_k=3$	0.91	0.98	1.00	0.97	0.98	0.99	0.95	0.97	1.00		$\beta_k=3$	0.88	0.93	0.91	0.88	0.87	0.84	0.98	0.94	1.00		$\beta_k=3$	0.88	0.93	0.91	0.88	0.87	0.84	0.98	0.94	1.00

		$\alpha_n=1$			$\alpha_n=2$			$\alpha_n=3$					$\alpha_n=1$			$\alpha_n=2$			$\alpha_n=3$													
		$\beta_k=1$	$\beta_k=2$	$\beta_k=3$	$\beta_k=1$	$\beta_k=2$	$\beta_k=3$	$\beta_k=1$	$\beta_k=2$	$\beta_k=3$			$\beta_k=1$	$\beta_k=2$	$\beta_k=3$	$\beta_k=1$	$\beta_k=2$	$\beta_k=3$	$\beta_k=1$	$\beta_k=2$	$\beta_k=3$											
$\alpha_n=1$	$\beta_k=1$	1.00									(c)	$\alpha_n=1$	$\beta_k=1$	1.00									(d)									
	$\beta_k=2$	0.96	1.00	0.94									$\beta_k=2$	0.97	1.00	0.96						$\beta_k=2$		0.97	1.00	0.96						
	$\beta_k=3$	0.98	0.94	1.00									$\beta_k=3$	0.96	0.96	1.00						$\beta_k=3$		0.96	0.96	1.00						
$\alpha_n=2$	$\beta_k=1$	0.47	0.52	0.49	1.00						$\alpha_n=2$	$\beta_k=1$	0.36	0.36	0.34	1.00						$\alpha_n=2$	$\beta_k=1$	0.36	0.36	0.34	1.00					
	$\beta_k=2$	0.49	0.54	0.52	0.95	1.00	0.95					$\beta_k=2$	0.33	0.34	0.31	0.96	1.00	1.00			$\beta_k=2$		0.33	0.34	0.31	0.96	1.00	1.00				
	$\beta_k=3$	0.47	0.51	0.49	0.97	0.95	1.00					$\beta_k=3$	0.32	0.33	0.30	0.96	1.00	1.00			$\beta_k=3$		0.32	0.33	0.30	0.96	1.00	1.00				
$\alpha_n=3$	$\beta_k=1$	0.76	0.74	0.79	0.39	0.43	0.39	1.00			$\alpha_n=3$	$\beta_k=1$	0.65	0.67	0.65	0.32	0.28	0.28	1.00			$\alpha_n=3$	$\beta_k=1$	0.65	0.67	0.65	0.32	0.28	0.28	1.00		
	$\beta_k=2$	0.73	0.73	0.75	0.40	0.44	0.41	0.95	1.00	0.92		$\beta_k=2$	0.66	0.67	0.68	0.28	0.24	0.24	0.90	1.00	0.96		$\beta_k=2$	0.66	0.67	0.68	0.28	0.24	0.24	0.90	1.00	0.96
	$\beta_k=3$	0.68	0.68	0.70	0.43	0.46	0.43	0.90	0.92	1.00		$\beta_k=3$	0.64	0.64	0.65	0.30	0.26	0.25	0.91	0.96	1.00		$\beta_k=3$	0.64	0.64	0.65	0.30	0.26	0.25	0.91	0.96	1.00

The tables show that the level of correlation between the models of different global permeability realisations (α_n) decreases as the value of K_{mult} increases. This means that for a lower value of K_{mult} (lesser heterogeneity), there was more correlation between the fluid displacement and production patterns regardless of the realisation of near-well perturbations applied. This was because of the low level of reservoir heterogeneity imposed in these model by the corresponding lower values of K_{mult} . Therefore, in models with high K_{mult} , the effects of reservoir heterogeneity or layering exerted a more dominant effect on the displacement process than viscous fingering or physical diffusion. For example, the fluid production profiles obtained from the models formed when $K_{mult} = 0.01$ (shown in Table 7(a)) were more correlated than those of the other models due to the similarity of these models imposed by the low value of the permeability multiplier.

As the reservoir heterogeneity increased, there was little correlation between the models of different global permeability realisations, particularly when $K_{mult} = 1.50$ (see Table 7(d)). A good level of correlation was only observed for models obtained from the same permeability realisation, α_n . As earlier mentioned, the use of the larger values of K_{mult} produced models with higher heterogeneities that have similar fingering behaviours and

fluid production profiles. Thus, the effects of viscous forces were very dominant in models with lower values of K_{mult} , and less dominant in models with high K_{mult} values regardless of the realisation of near-well perturbations.

In summary, as the heterogeneity imposed on the system increased, the effect of viscous fingering and diffusive forces decreased, although this effect cannot be totally eliminated. When viscous fingering forces are strong such as in cases with a high mobility ratio, a combination of viscous and diffusive forces and heterogeneity influence the fluid flow in the porous media regardless of the level of permeability heterogeneity.

4 Summary and Conclusions

The efficiency of miscible CO₂ enhanced oil recovery is a function of the small-scale local and field-scale areal and/or vertical sweep performance. The macroscopic sweep performance is a function of channelling caused by reservoir heterogeneity while microscopic sweep is a function of viscous fingering at the small scale. In field-scale simulations of miscible displacements, the effects of viscous fingering are ignored because of the computational requirements of fine grid simulations and the complexities associated with the fine-scale structure of the gas fingers and the miscible front.

In this study, we examined the interactions of viscous fingering and diffusive forces, and heterogeneity effects in miscible CO₂ enhanced oil recovery and storage using a set of homogeneous and layered heterogeneous inter-well scale 2D fine models. The use of these fine models provided an excellent tool for capturing of the effects of physical diffusion, viscous fingering, and channelling of the injected gas, and their impact on the performance of the CO₂ flooding. We aimed to identify the range of permeability heterogeneity at which viscous fingering forces have an insignificant effect on the fluid displacement and the overall performance of the flood, and at which the displacement was entirely dominated by the permeability variation within the reservoir rock. Our results showed that in models with little or no heterogeneity, the viscosity contrast between CO₂ and the resident oil exerted an important control on the spatial structure of the injected gas and on the performance of the flooding process at the very early and early fingering times, while the diffusive forces dominated at later times.

On the other hand, as degree of heterogeneity of the model increased, the impact of viscous fingering on the performance of the flooding process was observed to diminish, and that of gas channelling due to the presence of high permeability layers (or heterogeneity) increased. In porous media with very high degree of heterogeneity, the effect of viscous fingering was very minimal, and permeability heterogeneity exerted a total control on the performance of the flood. However, for very high degrees of perturbation or when the viscosity or mobility contrast between the resident and injected fluids is relatively large, the effect of the resulting viscous fingers would still be prominent irrespective of the level of heterogeneity of the porous media, even in the presence of significant heterogeneity. In these cases, a combination of viscous forces and heterogeneity dominates the flow behaviour. Overall, oil recovery during miscible CO₂ EOR was improved because of the interplay of the effects of viscous fingering/diffusion and reservoir heterogeneity.

In conclusion, this study buttresses the need for adequate knowledge of the layering patterns within a porous media. In cases where there is a lack of proper knowledge of the layering and/or the internal structure of the reservoir such as when well logging data are absent or are not properly correlated, this study provides a justification for accounting for the effects of layering as uncertain in the numerical modelling and/or reservoir optimisation studies. The methodology and results of this study can also be extended to immiscible and miscible injection studies in other GeoEnergy systems such as saline aquifers, geothermal reservoirs, and so on.

Acknowledgements

The authors wish to appreciate the Petroleum Technology Development Fund (PTDF) for funding this study. Schlumberger is also acknowledged for the provision of the ECLIPSE 300 simulator used in this study.

Data availability

The datasets generated during and/or analysed during the current study are available from the corresponding author on reasonable request.

Funding and/or conflicts of interests/competing interests

The work was funded by the Petroleum Technology Development Fund (PTDF), Grant No.: PTDF/ED/PHD /OP/1348/18.

5 References

- Abdul Hamid, S. A., & Muggeridge, A. (2018). Viscous fingering in reservoirs with long aspect ratios. *Proceedings - SPE Symposium on Improved Oil Recovery, 2018-April*(April), 14–18. <https://doi.org/10.2118/190294-ms>
- Abdul Hamid, S. A., & Muggeridge, A. H. (2020). Fingering regimes in unstable miscible displacements. *Physics of Fluids*, 32(1). <https://doi.org/10.1063/1.5128338>
- Aghdam, K. A., Moghaddas, J. S., Moradi, B., Dabiri, M., & Hassanzadeh, M. (2013). Maximizing the oil recovery through miscible Water Alternating Gas (WAG) injection in an Iranian oil reservoir. *Petroleum Science and Technology*, 31(22), 2431–2440. <https://doi.org/10.1080/10916466.2011.569822>
- Al-Mudhafar, W. J., Rao, D. N., & Srinivasan, S. (2018). Robust Optimization of Cyclic CO₂ flooding through the Gas-Assisted Gravity Drainage process under geological uncertainties. *Journal of Petroleum Science and Engineering*, 166(March), 490–509. <https://doi.org/10.1016/j.petrol.2018.03.044>
- Blackwell, R. J., Rayne, J. R., & Terry, W. M. (1959). Factors Influencing the Efficiency of Miscible Displacement. *Transactions of the AIME*, 217(01), 1–8. <https://doi.org/10.2118/1131-G>
- Blunt, M., Fayers, F. J., & Orr, F. M. (1993). Carbon dioxide in enhanced oil recovery. *Energy Conversion and Management*. [https://doi.org/10.1016/0196-8904\(93\)90069-M](https://doi.org/10.1016/0196-8904(93)90069-M)
- Booth, R. J. S. (2010). On the growth of the mixing zone in miscible viscous fingering. *Journal of Fluid Mechanics*, 655, 527–539. <https://doi.org/10.1017/S0022112010001734>
- Brock, D. C., & Orr Jr., F. M. (1991). Flow Visualization of Viscous Fingering in Heterogeneous Porous Media. In *SPE Annual Technical Conference and Exhibition* (p. SPE-22614-MS). <https://doi.org/10.2118/22614-MS>
- Chang, Y.-B., Lim, M. T., Pope, G. A., & Sepehrnoori, K. (1994). CO₂ flow patterns under multiphase flow: heterogeneous field-scale conditions. *SPE Reservoir Engineering (Society of Petroleum Engineers)*, 9(3), 208 – 216. <https://doi.org/10.2118/22654-pa>
- Chen, Z., Huan, G., & Ma, Y. (2006). *Computational Methods for Multiphase Flows in Porous Media*. Society for Industrial and Applied Mathematics. <https://doi.org/10.1137/1.9780898718942>
- Christie, M. A., & Bond, D. J. (1987). Detailed Simulation of Unstable Processes in Miscible Flooding. *SPE Reservoir Engineering (Society of Petroleum Engineers)*, 2(4), 514–522. <https://doi.org/10.2118/14896-PA>

- Christie, M. A., Muggeridge, A. H., & Barley, J. J. (1993). 3D Simulation of Viscous Fingering and WAG Schemes. *SPE Reservoir Engineering*, 8(01), 19–26. <https://doi.org/10.2118/21238-PA>
- Claridge, E. L. (1972). Prediction of Recovery in Unstable Miscible Flooding. *Society of Petroleum Engineers Journal*, 12(02), 143–155. <https://doi.org/10.2118/2930-PA>
- Esmail, T., Fallah Bolandtaba, S., & van Kruisdijk, cor. (2007). *Determination of WAG Ratios and Slug Sizes Under Uncertainty in a Smart Wells Environment*. <https://doi.org/10.2523/93569-ms>
- Ghaderi, S. M., Clarkson, C. R., Taheri, S., & Chen, S. (2013). Investigation of Economic Uncertainties of CO₂ EOR and Sequestration in Tight Oil Formations. *SPE Enhanced Oil Recovery Conference, Bachu 2003*. <https://doi.org/10.2118/165301-MS>
- Glasø, Ø. (1985). Generalized Minimum Miscibility Pressure Correlation. *Society of Petroleum Engineers Journal*, 25(06), 927–934. <https://doi.org/10.2118/12893-PA>
- Jaber, A. K., & Awang, M. B. (2017). Field-scale investigation of different miscible CO₂ -injection modes to improve oil recovery in a clastic highly heterogeneous reservoir. *Journal of Petroleum Exploration and Production Technology*, 7(1), 125–146. <https://doi.org/10.1007/s13202-016-0255-5>
- Jangir, P., Mohan, R., & Chokshi, P. (2022). Experimental study on the role of polymer addition in Saffman-Taylor instability in miscible flow displacement. *Physics of Fluids*, 34(9). <https://doi.org/10.1063/5.0102237>
- Koval, E. J. (1963). A Method for Predicting the Performance of Unstable Miscible Displacement in Heterogeneous Media. *Society of Petroleum Engineers Journal*, 3(02), 145–154. <https://doi.org/10.2118/450-PA>
- Luo, H., Mohanty, K. K., & Delshad, M. (2017). Modeling and upscaling unstable water and polymer floods: Dynamic characterization of the effective viscous fingering. *SPE Reservoir Evaluation and Engineering*, 20(4), 779–794. <https://doi.org/10.2118/179648-pa>
- Malhotra, S., Sharma, M. M., & Lehman, E. R. (2015). Experimental study of the growth of mixing zone in miscible viscous fingering. *Physics of Fluids*, 27(1). <https://doi.org/10.1063/1.4905581>
- Moghadas, R., Rostami, A., & Hemmati-Sarapardeh, A. (2018). Enhanced Oil Recovery Using CO₂. In *Fundamentals of Enhanced Oil and Gas Recovery from Conventional and Unconventional Reservoirs*. <https://doi.org/10.1016/b978-0-12-813027-8.00003-5>
- Moortgat, J., Li, Z., & Firoozabadi, A. (2012). Three-phase compositional modeling of CO₂ injection by higher-order finite element methods with CPA equation of state for aqueous phase. *Water Resources Research*, 48(12). <https://doi.org/10.1029/2011WR011736>
- Naderi, S., & Simjoo, M. (2019). Numerical study of Low Salinity Water Alternating CO₂ injection for enhancing oil recovery in a sandstone reservoir: Coupled geochemical and fluid flow modeling. *Journal of Petroleum Science and Engineering*, 173(October 2018), 279–286. <https://doi.org/10.1016/j.petrol.2018.10.009>
- Nijjer, J. S., Hewitt, D. R., & Neufeld, J. A. (2018). The dynamics of miscible viscous fingering from onset to shutdown. *Journal of Fluid Mechanics*, 837, 520–545. <https://doi.org/10.1017/jfm.2017.829>
- Orr, F. M. (2004). Storage of Carbon Dioxide in Geologic Formations. *Journal of Petroleum Technology*, 56(09), 90–97. <https://doi.org/10.2118/88842-JPT>
- Peaceman, D. W., & Rachford Jr., H. H. (1962). Numerical Calculation of Multidimensional Miscible Displacement. *Society of Petroleum Engineers Journal*, 2(04), 327–339. <https://doi.org/10.2118/471-PA>
- Perkins, T. K., & Johnston, O. C. (1963). A Review of Diffusion and Dispersion in Porous Media. *Society of Petroleum Engineers Journal*, 3(01), 70–84. <https://doi.org/10.2118/480-pa>

- Peters, E. J., Broman Jr., W. H., & Broman, J. A. (1984). A Stability Theory for Miscible Displacement. In *SPE Annual Technical Conference and Exhibition* (p. SPE-13167-MS). <https://doi.org/10.2118/13167-MS>
- Stewart, R. J., Johnson, G., Heinemann, N., Wilkinson, M., & Haszeldine, R. S. (2018a). Low carbon oil production: Enhanced oil recovery with CO₂ from North Sea residual oil zones. *International Journal of Greenhouse Gas Control*, 75(February), 235–242. <https://doi.org/10.1016/j.ijggc.2018.06.009>
- Stewart, R. J., Johnson, G., Heinemann, N., Wilkinson, M., & Haszeldine, R. S. (2018b). Low carbon oil production: Enhanced oil recovery with CO₂ from North Sea residual oil zones. *International Journal of Greenhouse Gas Control*. <https://doi.org/10.1016/j.ijggc.2018.06.009>
- Tan, C. T., & Homsy, G. M. (1986). Stability of miscible displacements in porous media: rectilinear flow. *Phys. Fluids*, 29(11, Nov. 1986), 3549–3556. <https://doi.org/10.1063/1.865832>
- Tchelepi, H. A., & Orr, F. M. (1994). Interaction of viscous fingering, permeability heterogeneity, and gravity segregation in three dimensions. *SPE Reservoir Engineering (Society of Petroleum Engineers)*, 9(4), 266–271. <https://doi.org/10.2118/25235-PA>
- Tchelepi, H. A., Orr, F. M., Rakotomalala, N., Salin, D., & Wouméni, R. (1993). Dispersion, permeability heterogeneity, and viscous fingering: Acoustic experimental observations and particle-tracking simulations. *Physics of Fluids A: Fluid Dynamics*, 5(7), 1558–1574. <https://doi.org/10.1063/1.858833>
- Vahidi, A., Ahmadi, M., & Nourmohammad, A. (2014). Carbon Dioxide Minimum Miscibility Pressure Estimation (Case Study). *Journal of Petroleum Science and Technology*, 4(2), 20–27.
- Zahoor, M. K., Derahman, M. N., & Yunan, M. H. (2011). Wag Process Design – an Updated Review. *Brazilian Journal of Petroleum and Gas*, 5(2), 109–121. <https://doi.org/10.5419/bjpg2011-0012>
- Zimmerman, W. B., & Homsy, G. M. (1991). Nonlinear viscous fingering in miscible displacement with anisotropic dispersion. *Physics of Fluids A: Fluid Dynamics*, 3(8), 1859–1872. <https://doi.org/10.1063/1.857916>
- Zimmerman, W. B., & Homsy, G. M. (1992). Viscous fingering in miscible displacements: Unification of effects of viscosity contrast, anisotropic dispersion, and velocity dependence of dispersion on nonlinear finger propagation. *Physics of Fluids A: Fluid Dynamics*, 4(11), 2348–2359. <https://doi.org/10.1063/1.858476>

Statements & Declarations

Funding: This work was supported by the Petroleum Technology Development Fund (PTDF). P. Ogbeiwi received funding from the Petroleum Technology Development Fund (PTDF); **Competing Interests:** The authors have no relevant financial or non-financial interests to disclose; **Author Contributions:** Precious Ogbeiwi contributed to the conceptualisation, formal analysis, methodology, software, and writing - original draft. Karl D. Stephen contributed to the conceptualisation, supervision, writing - review & editing, software, visualisation, and validation; **Data Availability:** The datasets generated during and/or analysed during the current study are available from the corresponding author on reasonable request.